

Determining the axial direction of high-shear flux transfer events: Implications for models of FTE structure

R. C. Fear¹, S. E. Milan¹, K. Oksavik²

18th September 2012

An edited version of this paper was published by AGU.

Copyright (2012) American Geophysical Union.

Citation: Fear, R. C., S. E. Milan and K. Oksavik (2012), Determining the axial direction of high-shear flux transfer events: Implications for models of FTE structure, *J. Geophys. Res.*, **117**, A09220, doi:10.1029/2012JA017831.

¹Department of Physics & Astronomy, University of Leicester, Leicester, LE1 7RH, United Kingdom

²Department of Physics & Technology, University of Bergen, P.B. 7803, NO-5020 Bergen, Norway

Correspondence to: r.fear@ion.le.ac.uk

Abstract

Flux transfer events are bursts of dayside reconnection, which give rise to local perturbations of the magnetic field that can be observed by spacecraft near the magnetopause. Although it is commonly accepted that flux transfer events are caused by reconnection, various models exist to explain their structure. A key difference between mechanisms is that when the magnetic shear across the magnetopause is close to 180° , some models will give rise to a structure whose axis is oriented north-south, whereas others will result in a dawn-dusk oriented structure. Several techniques for determining the axial direction of such structures have been suggested: minimum variance analysis on the magnetic field, minimization of the axial electric field, and Grad Shafranov reconstruction. We apply these techniques to a series of flux transfer events observed by Cluster at a high-shear magnetopause crossing on 27th March 2007. Minimum variance analysis on the signatures caused by the draping of unconnected magnetic flux around the flux transfer events consistently results in an axial direction which is directed dawn-dusk. However, the electric field technique, applied to flux transfer events which are penetrated by the spacecraft, results in a mixture of north-south and dawn-dusk axes. Testing these axial directions with Grad Shafranov reconstruction suggests that the axes of events which appear to be oriented dawn-dusk might be more reliably determined than the axes of events which appear to be north-south. Using the Grad Shafranov method alone to determine the axial direction of the penetrated events gives dawn-dusk axial directions, consistent with the results of minimum variance analysis on the draping events. Overall, these observations are consistent with the formation of flux transfer events by processes involving relatively long reconnection lines (e.g. single or multiple X-line reconnection) rather than as an elbow-shaped flux tubes as originally envisaged. Furthermore, examination of one particular flux transfer event that was observed by Cluster 1 but not by Cluster 2 (which was closer to the magnetopause), allows us to preclude the elbow-shaped model for this event.

1 Introduction

Since the discovery of in situ flux transfer event (FTE) signatures by *Russell and Elphic* (1978, 1979), several conceptual models have been proposed to explain their characteristic magnetic field and plasma variations. *Russell and Elphic* (1978) proposed an elbow-shaped flux tube model, where FTE structures were formed by a localized patch of reconnection, resulting in a pair of flux tubes that are broadly oriented north-south when the interplanetary magnetic field (IMF) is strongly southward. Subsequently, *Lee and Fu* (1985) proposed that multiple X-lines, which could be significantly longer than in the elbow-shaped flux tube model, could form east-west oriented flux tubes which could give rise to the same signatures. *Southwood et al.* (1988) and *Scholer* (1988) suggested that bulges could form in the magnetopause boundary layer as a result of the increased thermal pressure of plasma heated by a burst of reconnection at a single X-line, which again could be either long or short (the ‘single X-line’ model). These bulges do not form flux ropes, but still replicate the observed signatures and have the same axial orientation as multiple X-line flux ropes. (See also *Scholer* (1995), *Lockwood and Hapgood* (1998) and *Fear et al.* (2008) for further explanations of these and other FTE models.)

A few authors have examined the differences between these models; *Lockwood and Hapgood* (1998) found that the continuous variation in the ion distribution observed within one example FTE was consistent with the passage through open magnetic field lines corresponding to varying elapsed times since reconnection, which they concluded was consistent with the single X-line model and not the elbow-shaped flux tube model. By considering other plasma signatures observed during this event, they also excluded the multiple X-line mechanism as the cause for this FTE. Observations of the velocities of larger-scale FTEs observed several Earth radii from the subsolar point (*Fear et al.*, 2007) have been more consistent with the velocity expected of open magnetic field lines (*Cowley and Owen*, 1989; *Cooling et al.*, 2001) than the magnetosheath velocity, suggestive of the single X-line or elbow-shaped flux tube mechanism. However, other studies based on reconstruction techniques (*Sonnerup et al.*, 2004; *Hasegawa et al.*, 2006), modeled/observed seasonal dependencies (*Raeder*, 2006; *Korotova et al.*, 2008; *Fear et al.*, 2012), comparison of the modeled/observed details of FTE signatures (*Ku and Sibeck*, 1997, 1998a,b, 2000; *Fear et al.*, 2010a) and case studies (*Hasegawa et al.*, 2010; *Øieroset et al.*, 2011) suggest a multiple X-line mechanism. (It might also be that the shear-driven 3D reconnection generation mechanism described by *Dorelli and Bhattacharjee* (2009) could explain some of the above observations, such as the observed bias towards FTE signatures being observed in the winter hemisphere; however *Dorelli and Bhattacharjee* (2009) only considered equinoctial conditions, so no conclusions about seasonal bias can be drawn from their work yet [J. Dorelli, private communication].) *Hasegawa et al.* (2010) and *Øieroset et al.* (2011) reported converging reconnection jets either side of an FTE, indicating the presence of nearby X-lines on each side. Both events were magnetosheath FTEs; *Hasegawa et al.* (2010) also reported a heated magnetosheath electron population both parallel and antiparallel to the magnetic field direction, which is inconsistent with a single X-line geometry (unless some other process causes the mirroring of the heated plasma) given the location of the spacecraft outside the magnetopause. However, bidirectional magnetosheath electron signatures appear to be common features of magnetosheath FTEs (*Robert et al.*, 2006; *Fear et al.*, 2007).

The elbow-shaped flux tube model is necessarily patchy, whereas the single and multiple X-line model structures may either be very localized or may extend over a significant portion of the magnetopause, explaining large-scale ionospheric signatures of FTEs such as those observed by *Milan et al.* (2000) as well as smaller-scale ionospheric signatures (e.g. *Marchaudon et al.*, 2004; *Oksavik et al.*, 2004, 2005). One way to investigate the in situ extent of FTE signatures is to use data from magnetopause crossings made by the four Cluster spacecraft since 2006, as they have regularly crossed the magnetopause with inter-spacecraft separations of the order of 10,000 km. Such a separation is large enough to observe macroscale differences between the signatures observed at the four spacecraft, but small enough to be confident that all spacecraft are observing the same FTE structure rather than another nearby event. *Fear et al.* (2008) determined the poleward and minimum azimuthal scale sizes of a series of FTEs; whilst they found that the FTEs clearly had minimum azimuthal scales that were greater than their poleward scale sizes, the relatively low shear between the magnetosheath and magnetospheric magnetic fields ($\sim 100^\circ$) meant that these structures could still be consistent with the elbow-shaped model. Therefore, it is of interest to examine magnetopause crossings which occur when the magnetic shear is much closer to 180° . Under these circumstances, the orientation of the flux tube/bulge structure should be largely north-south in the elbow-shaped flux tube model, and dawn-dusk in the single and multiple X-line models

(Sonnerup, 1988). Therefore, Fear et al. (2010b) applied the same multi-spacecraft techniques to FTEs observed on a magnetopause crossing in March 2007, which occurred near noon MLT and during which the lagged IMF was mostly strongly southward, resulting in a high magnetic shear at the magnetopause. The separation of the spacecraft was smaller than in the previous case study ($\sim 8,500$ km), reducing the minimum azimuthal scale size that can be inferred from the spacecraft separation. Whilst some signatures were observed at all four spacecraft and had a minimum azimuthal scale size which was comparable to or greater than the poleward size (as far as could be deduced from the slightly smaller tetrahedron), interestingly other signatures were observed at only subsets of the spacecraft. Since all four spacecraft were oriented close to a plane that was tangential to the magnetopause, and all four spacecraft crossed the magnetopause once only and within 4 minutes of each other, this suggests that some of the FTE structures were much patchier.

The object of this paper is to take advantage of the high magnetic shear at the magnetopause during the interval studied by Fear et al. (2010b), which implies a 90° difference between the axial direction predicted by the elbow-shaped flux tube model on one hand and the single and multiple X-line models on the other, to deduce the axial directions of the FTE structures (particularly for the patchy events). Fear et al. (2010b) showed that the larger-scale structures (observed by all four spacecraft) had velocities which were strongly poleward, indicative of axes that are directed azimuthally. However, there were evident variations between some signatures observed at the four spacecraft, and multi-spacecraft comparisons do not allow conclusions about the orientation of patchy events. Therefore, in this study we will use single-spacecraft methods to determine the axial direction. Several such methods have been suggested, which will be discussed in the following section. In Section 3, we briefly outline the instrumentation used in this study. In Section 4, we provide an overview of FTEs observed by Fear et al. (2010b), and apply the single spacecraft methods to these FTEs in Section 5. We will then compare the results from the different methods, discuss our findings and summarize our conclusions.

2 Single-spacecraft methods

2.1 Minimum variance analysis

Minimum variance analysis (MVA) (Sonnerup and Scheible, 1998, and references therein) is a technique that is applied to a vector time series to find the directions in which the component of the vector varies the least and the most (the minimum and maximum variance directions). The minimum and maximum variance directions are orthogonal to each other, and the direction that is orthogonal to both is referred to as the intermediate variance direction. These directions are found by solving an eigenvalue equation which is given as Equation 8.7 in Sonnerup and Scheible (1998). The eigenvectors $\hat{\mathbf{x}}_1$, $\hat{\mathbf{x}}_2$ and $\hat{\mathbf{x}}_3$, corresponding to eigenvalues λ_1 , λ_2 and λ_3 (where $\lambda_1 > \lambda_2 > \lambda_3$) give the maximum, intermediate and minimum variance directions.

Minimum variance analysis on magnetic field data is commonly used to determine the normal to rotational and tangential discontinuities such as the magnetopause current layer (e.g. Sonnerup and Cahill, 1967), but several studies have applied the same mathematical technique to determine the axial direction of flux ropes at the magnetopause, in the magnetotail and in the Venusian ionosphere (e.g. Sibeck et al., 1984; Elphic et al., 1980; Elphic and Russell, 1983; Farrugia et al., 1987; Slavin et al., 1989; Zong et al., 1997). The eigenvector which corresponds to the axial direction depends upon the model that is assumed for the flux rope structure and on the depth of the crossing (measured by the impact parameter, which is defined as the smallest distance between the spacecraft track and the flux rope axis). Several studies have considered flux ropes with a strong axial core field, and where the spacecraft crossed close to the center of the flux rope (i.e. with a small impact parameter) (e.g. Sibeck et al., 1984; Elphic and Russell, 1983; Zong et al., 1997). In these studies, the maximum variance direction has been taken to be the axial direction, due to the strength of the axis-aligned core field. Slavin et al. (1989) modeled force-free flux ropes, and found that the axial direction corresponded to the intermediate direction due to the relatively weak axial magnetic field. Farrugia et al. (1987) modeled the draping of magnetic flux around a cylinder, assuming incompressible plasma flow around the cylinder, and found that the component of the draped field that was along the axial direction was constant. Consequently, if MVA is applied to a ‘draping’ FTE signature (where there is no electron or ion signature, indicating that the spacecraft did not cross onto open magnetic field lines, or come within two electron gyroradii of doing

so (e.g. *Oksavik et al.*, 2002)), then the minimum variance direction should be parallel or antiparallel to the axial direction.

Walthour et al. (1993, 1994) and *Khrabrov and Sonnerup* (1998) investigated the effect of removing the incompressible flow assumption and found a relatively simple expression for an angle by which the minimum variance eigenvector should be rotated to produce an estimate of the axial direction which accounts for the compressibility of the plasma. They showed that if a spacecraft observed only the draping of flux around an FTE, the unperturbed magnetic field outside the FTE (\mathbf{B}_0) was approximately equal to the mean magnetic field during the passage of the structure ($\langle \mathbf{B} \rangle$), and the maximum and intermediate eigenvalues were well determined with respect to each other, then the magnetopause normal should be well approximated by either the maximum or the intermediate eigenvector and the true axial direction should be given by a clockwise rotation of the minimum eigenvector by an angle θ_N about the eigenvector which approximates the normal. If the maximum eigenvector approximates the normal (Case 1), then:

$$\tan \theta_N = \tan \psi (\lambda_2 / \lambda_1 - 1) \quad (1)$$

where $\tan \psi = (\mathbf{B}_0 \cdot \hat{\mathbf{x}}_3) / (\mathbf{B}_0 \cdot \hat{\mathbf{x}}_2)$ and $\lambda_1 > \lambda_2 \gg \lambda_3$. If the intermediate eigenvector approximates the normal (Case 2), then the rotation is given by:

$$\tan \theta_N = \tan \psi (\lambda_1 / \lambda_2 - 1) \quad (2)$$

where $\tan \psi = (\mathbf{B}_0 \cdot \hat{\mathbf{x}}_3) / (-\mathbf{B}_0 \cdot \hat{\mathbf{x}}_1)$. In the case where $\lambda_1 \approx \lambda_2$, the maximum and intermediate eigenvectors are poorly determined, but this situation corresponds to $\theta_N \approx 0$.

More recently, *Xiao et al.* (2004) have modeled force-free and strong-core-field flux ropes, and carried out minimum variance analysis on the magnetic field observed by various virtual satellites at a range of impact parameters. If the satellite passes through a force-free flux rope (e.g. *Slavin et al.*, 1989), then *Xiao et al.* (2004) found that the intermediate variance direction was indeed the best predictor of the axial direction, but the difference between the intermediate direction and the true axial direction was up to 20°. When the satellite passes through a flux rope with a primarily axis-aligned current (i.e. non-force-free) then *Xiao et al.* (2004) found that the maximum variance direction best predicted the axial direction for crossings with small impact parameters, and the intermediate variance direction best predicted it for crossings with larger impact parameters, but in both cases there was a difference between the MVA direction and the true axial direction of 20-30°. In the case of non-force-free flux ropes, more accurate determinations of the axis were obtained by carrying out MVA on the current structure.

2.2 Grad Shafranov method

Grad Shafranov reconstruction is a technique that has been proposed to reconstruct two dimensional magnetic field structures from time series data taken from a satellite pass through the structure (*Hau and Sonnerup*, 1999; *Hu and Sonnerup*, 2003; *Sonnerup et al.*, 2004, 2006; *Hasegawa et al.*, 2005, 2006). The technique makes several assumptions. Firstly, it is assumed that the structure is approximately two dimensional (defining the $\hat{\mathbf{x}}\text{-}\hat{\mathbf{y}}$ plane, where $\hat{\mathbf{x}}$ is along the direction of the spacecraft's path), such that spatial changes out of the 2D plane (referred to as the invariant axis $\hat{\mathbf{z}}$) are much more gradual than within the plane. Secondly, a frame of reference must exist in which the structure is approximately stationary. (This frame is called the "proper frame", which is a generalization of the de Hoffmann-Teller [dHT] frame (*De Hoffmann and Teller*, 1950).) Thirdly, it is assumed that inertia effects can be neglected. If the 2D criterion is met, then the magnetic field can be expressed in terms of the vector potential $\mathbf{A} = A(x, y)\hat{\mathbf{z}}$ (*Hau and Sonnerup*, 1999):

$$\mathbf{B} = (\partial A / \partial y, -\partial A / \partial x, B_z(x, y)) \quad (3)$$

The component of the vector potential along the spacecraft track can be obtained by integrating the component of the magnetic field that is perpendicular to both the selected invariant axis and the spacecraft track:

$$A(x, 0) = - \int_0^x B_y(x, 0) dx = |\mathbf{V}_{HT}| \int_0^t B_y(t) dt \quad (4)$$

If the structure is in magnetohydrostatic equilibrium, then the pressure gradient balances the magnetic tension transverse to the magnetic field ($\nabla_t p = (\mathbf{j} \times \mathbf{B})_t$). Under the 2D assumption, this reduces to the Grad-Shafranov equation:

$$\frac{\partial^2 A}{\partial x^2} + \frac{\partial^2 A}{\partial y^2} = -\mu_0 \frac{dP_t}{dA} = -\mu_0 j_z \quad (5)$$

where $P_t = (p + B_z^2/2\mu_0)$ is the transverse pressure, and the plasma pressure p and the axial magnetic field component B_z are functions of A alone.

In this study we will not apply the full reconstruction method; we simply take advantage of the assumption that the plasma pressure and axial magnetic field component should be functions of $A(x, y)$ alone. We vary our choice of trial axis direction, and find the direction which best orders the relationship between the plasma pressure and axial field component and A , as suggested by *Hau and Sonnerup (1999)*.

2.3 Faraday's Law method

Sonnerup and Hasegawa (2005) presented a new method to determine the axial direction of a flux rope, based on Faraday's Law. Their method requires the spacecraft to observe the flux rope itself (not just the draping of flux around it). Like the Grad Shafranov method, it assumes that the flux rope structure is essentially two dimensional and that the flux rope is in hydrostatic equilibrium. Under these conditions, the theta component of Faraday's law, expressed in cylindrical coordinates, gives $\partial E_z / \partial r = 0$, where $\hat{\mathbf{z}}$ is again the invariant axis direction. *Sonnerup and Hasegawa (2005)* then outlined a method to find the rest frame and axial direction which satisfy these conditions, by finding the eigenvectors of the matrix:

$$\mathbf{M}_0 = -\mathbf{M}^{EB} \cdot \mathbf{M}^{-BB} \cdot \mathbf{M}^{BE} + \mathbf{M}^{EE} \quad (6)$$

where the covariance matrices $\mathbf{M}^{EB} = \langle \delta \mathbf{E} \delta \mathbf{B} \rangle$, $\mathbf{M}^{BE} = \langle \delta \mathbf{B} \delta \mathbf{E} \rangle$, $\mathbf{M}^{EE} = \langle \delta \mathbf{E} \delta \mathbf{E} \rangle$ and $\mathbf{M}^{BB} = \langle \delta \mathbf{B} \delta \mathbf{B} \rangle$ are constructed from the deviations of individual measurements of the electric and magnetic fields from their means ($\delta \mathbf{E} = (\mathbf{E} - \langle \mathbf{E} \rangle)$ and $\delta \mathbf{B} = (\mathbf{B} - \langle \mathbf{B} \rangle)$), and \mathbf{M}^{-BB} is the inverse of \mathbf{M}^{BB} .

The eigenvalues and eigenvectors of \mathbf{M}_0 are found, and the minimum variance direction is taken to be the predictor of the true axial direction ($\hat{\mathbf{k}}$). The velocity of the structure is given by:

$$\mathbf{V}_0 = -\hat{\mathbf{k}} \times \mathbf{U}_0 \quad (7)$$

where:

$$\mathbf{U}_0 = -\mathbf{M}^{BB} \cdot \mathbf{M}^{BE} \cdot \hat{\mathbf{k}} \quad (8)$$

Sonnerup and Hasegawa (2005) discuss three quantitative indicators of how well the basic assumptions are satisfied: $\mathbf{U}_0 \cdot \hat{\mathbf{k}}$ should be small compared with $|\mathbf{U}_0|$, the minimum eigenvalue of \mathbf{M}_0 should be small, and the ratio of the intermediate to minimum eigenvalues should not be small. They applied this method to two flux transfer events which they had previously examined using Grad Shafranov reconstructions, and calculated axial directions which were in excellent agreement with Grad Shafranov axes. The minimum eigenvalues of \mathbf{M}_0 were 0.003 and 0.02 (mV/m)², and the ratios of the intermediate to minimum eigenvalues were 6.9 and 6.5. The ratios $\mathbf{U}_0 \cdot \hat{\mathbf{k}} / |\mathbf{U}_0|$ were -0.02 and -0.03. However, they cautioned that the Faraday's Law method can also fail to produce such good agreement, and so must be used carefully.

More recently, *Trenchi et al. (2011)* have also applied this method to a flux rope observed by the Double Star TC-1 satellite, calculating an axial direction that was within 3° of parallel to the orientation inferred of a nearby pair of reconnection lines, suggestive of one of the longer X-line mechanisms.

3 Instrumentation

In this paper, we seek to apply the methods outlined in the previous section to Cluster 1 and 2 observations of FTEs reported by *Fear et al. (2010b)*. All Cluster data are obtained from the Cluster Active Archive.

We make use of data from the Fluxgate Magnetometer (FGM) instruments (*Balogh et al., 2001; Gloag et al., 2010*) and the Plasma Electron and Current Experiment (PEACE) (*Johnstone et al., 1997*;

Fazakerley et al., 2010) on all four spacecraft to provide an overview of the interval, identify flux transfer event signatures and identify whether the spacecraft observes the FTE core and/or the draping region. For these purposes, we use spin resolution (~ 4 s) measurements of the magnetic field observed by FGM, and spin resolution pitch angle distributions from the PEACE instrument.

In order to calculate the FTE axial directions with the MVA method, we use FGM data at the highest resolution available (22.4 Hz).

The Faraday's Law method requires observations of the electric and magnetic fields in order to construct the matrix \mathbf{M}_0 (Equation 6). We obtain the electric field in two ways. On Cluster 1 it is found by taking the cross product of the observed ion velocity and the magnetic field ($\mathbf{E} = -\mathbf{v} \times \mathbf{B}$). The ion velocity is obtained from moments calculated onboard the spacecraft by the Hot Ion Analyzer on the Cluster Ion Spectrometry instrument (CIS-HIA) (Rème et al., 2001; Dandouras et al., 2010). HIA provides onboard moments, and hence a measure of the plasma bulk velocity, for each spacecraft spin (~ 4 s). Consequently we calculate \mathbf{E} using spin resolution HIA and FGM measurements. CIS data are unavailable from Cluster 2, but we use the electric field measured by the Electric Field and Wave (EFW) instrument (Gustafsson et al., 2001; Khotyaintsev et al., 2010). A 2D measurement of the electric field is made in the spin plane of the spacecraft at 25 Hz cadence. The third component is then calculated by assuming that there is no component of the electric field parallel to the magnetic field ($\mathbf{E} \cdot \mathbf{B} = 0$). In order to reduce the error on the computed electric field component, it is only calculated when the magnetic field vector is more than 15° out of the spin plane of the spacecraft and the magnitude of the component of the magnetic field out of the spin plane is larger than 2 nT.

The Grad Shafranov method requires the establishment of the de Hoffmann-Teller frame and calculation of the plasma pressure and magnetic field vector potential. Since ion measurements are unavailable from Cluster 2, this is applied only to data from Cluster 1. We use the ion velocity, density and parallel & perpendicular temperatures calculated from the HIA onboard moments and FGM data, both at spin resolution.

We use supporting IMF data from the OMNI high resolution data set (King and Papitashvili, 2005) which (for this interval) is based on observations by the Wind magnetic field instrument and solar wind experiment (Lepping et al., 1995; Ogilvie et al., 1995).

4 Interval overview

4.1 Cluster observations

On the 27th March 2007, the Cluster spacecraft crossed the dayside magnetopause near local noon and in the northern hemisphere, at $(9.2, -1.3, 2.8)_{GSM} R_E$. An overview of the interval is shown in Figure 1. The top panel shows the electron distribution observed by Cluster 2. Initially a hot, but relatively rarified distribution was observed, which indicates that the spacecraft was in the magnetosphere. After 05:05 UT, Cluster 2 observed a cooler, denser electron population which indicates that the spacecraft crossed the magnetopause at 05:05 UT and entered into the magnetosheath.

The next seven panels in Figure 1 show the magnetic field that was observed by all four spacecraft, plotted in boundary normal coordinates (Russell and Elphic, 1978). The $\hat{\mathbf{n}}$ component is directed normal to the local magnetopause surface, $\hat{\mathbf{I}}$ is within the plane defined by $\hat{\mathbf{n}}$ and directed poleward, and $\hat{\mathbf{m}}$ is directed downward. The boundary normal coordinate system was obtained independently for each spacecraft. The magnetopause normal direction was determined by carrying out minimum variance analysis on the full resolution magnetic field data as each spacecraft crossed the magnetopause. The azimuthal unit vector ($\hat{\mathbf{m}}$) was calculated by taking the cross product of the Earth's dipole moment with $\hat{\mathbf{n}}$ and normalizing the result, and $\hat{\mathbf{I}}$ is the cross product of $\hat{\mathbf{m}}$ and $\hat{\mathbf{n}}$. The interval used for MVA, the ratio of the intermediate to minimum eigenvalues and the minimum variance direction ($\hat{\mathbf{n}}$) for each spacecraft and the two other unit vectors are recorded in Table 1. The $\hat{\mathbf{I}}$ vectors are largely aligned along the Z_{GSE} direction, $\hat{\mathbf{m}}$ is largely along $-Y_{GSE}$ and $\hat{\mathbf{n}}$ is largely along X_{GSE} , consistent with the location of the spacecraft northward of the subsolar point.

The B_L component (Figure 1) was initially strongly positive at all four spacecraft ($B_L \approx +70$ nT). As Cluster 2 left the magnetosphere at 05:05 UT, it observed a decrease of B_L to approximately zero, followed by a further decrease to a strongly negative value ($B_L \approx -50$ nT). The time at which each spacecraft crossed the magnetopause can be determined from the reversal in the B_L component. Cluster 3 (green

trace) crossed the magnetopause at about the same time as Cluster 2, whereas Clusters 1 and 4 (black and blue traces respectively) crossed slightly later at 05:08 UT. This is consistent with the orientation of the Cluster tetrahedron, which is shown in the boundary normal coordinate system for Cluster 3 in Figure 2. The spacecraft were aligned in a plane, close to tangential to the nominal magnetopause; the maximum separation of the spacecraft in the $\hat{\mathbf{n}}$ direction was only 1,300 km, with Clusters 3 and 2 as the outermost spacecraft. Clusters 1 and 2 both lay poleward of Clusters 3 and 4, and Clusters 1 and 2 were the most azimuthally-separated spacecraft (i.e. they were furthest separated in the $\hat{\mathbf{m}}$ direction).

The reversal in B_L (Figure 1) was much more abrupt at Clusters 1 and 4 than at Clusters 2 and 3, indicating that Clusters 1 and 4 crossed the magnetopause much more quickly than Clusters 2 and 3. The latter two spacecraft appear to have crossed through a boundary layer between the magnetosphere-proper and the magnetosheath, in which a heated magnetosheath electron population was observed (top panel of Figure 1 for Cluster 2, not shown for Cluster 3) and there was a rapid oscillation of the B_N component. This period has been studied in more detail by *Laitinen et al.* (2010), who discussed the presence of reconnection jets in the magnetosheath and concluded that during the magnetopause crossing intervals reconnection continued in a quasi-continuous but non-steady manner.

Before the magnetopause crossings, the B_M components at all four spacecraft were all close to zero. Once the spacecraft had entered the magnetosheath, the B_M components remained small compared with B_L except between 05:15 and 05:25 UT, when the B_M components at all four spacecraft increased somewhat in magnitude.

The B_N components immediately before and after the magnetopause crossings were all close to zero, indicative of a successful determination of the magnetopause normals at all four spacecraft, except for a series of mostly positive-then-negative perturbations. These mainly bipolar B_N variations are the magnetopause signatures of standard polarity flux transfer events. There was a mixture of draping-only signatures without any electron signature (e.g. those observed before 04:58 UT) and ‘core’-crossing signatures which were accompanied by an electron signature (e.g. the signatures observed by Cluster 2 at 04:59 and 05:02 UT and most of the signatures observed in the magnetosheath).

The bottom panel of Figure 1 shows the angle in the $\hat{\mathbf{l}}\text{-}\hat{\mathbf{m}}$ plane made by the magnetic field vector observed by Cluster 2 (α_{LM}) in red, and the IMF clock angle (θ_{CA}) in brown. θ_{CA} was determined from the high resolution OMNI data (*King and Papitashvili*, 2005), which is discussed further below. α_{LM} remained close to 180° from the magnetopause crossing until 05:15 UT, aside from a couple of transient deviations associated with the passage of FTEs. Between 05:15 and 05:25 UT, α_{LM} reduced due to the enhancement in the magnitude of B_M .

4.2 IMF observations

The IMF from the OMNI data set is compared with the magnetosheath magnetic field in Figure 3. The top four panels of Figure 3 show the GSM components and magnitude of the IMF and magnetosheath magnetic field. (The magnetic field components observed by Cluster 2 are divided by 8 in order to compare more easily with the spacecraft situated in the solar wind). The fifth panel shows the angle α_{LM} from Figure 1 and the IMF clock angle (θ_{CA}). The following two panels show the Earthward component of the solar wind velocity and the solar wind dynamic pressure, and the bottom panel shows the auroral electrojet AU and AL indices.

The OMNI data set consists of IMF observations from various spacecraft which have been propagated to the nose of the bow shock as described by *King and Papitashvili* (2005). During this interval, the source of the OMNI IMF values was the Wind spacecraft, which was situated close to the Sun-Earth line at $(198, 10, -16)_{GSM} R_E$. In order to account for the propagation of plasma from the bow shock to the magnetopause, we apply an additional lag τ_{sh} to the OMNI data which we determine from Equation 3 of *Khan and Cowley* (1999):

$$\tau_{sh} = \frac{(R_{BS} - R_{MP})}{(V_{BS} - V_{MP})} \ln \left(\frac{V_{BS}}{V_{MP}} \right) \quad (9)$$

R_{BS} & R_{MP} are the subsolar positions of the bow shock and magnetopause and V_{BS} & V_{MP} are the magnetosheath flow speeds just downstream of the bow shock and immediately upstream of the magnetopause. Following *Khan and Cowley* (1999), we assume a value of V_{MP} (the inflow speed at a reconnection site at the magnetopause) of 20 km s^{-1} , and express V_{BS} in terms of the upstream solar wind speed ($V_{BS} = 0.28V_{SW}$). Since $V_{SW} \approx 470 \text{ km s}^{-1}$ during this interval (Figure 3), $V_{BS} = 130 \text{ km s}^{-1}$.

We use the same value of R_{BS} as that used in the propagation of the OMNI data to the bow shock, which is determined by *King and Papitashvili* (2005) using the *Farris and Russell* (1994) model ($11.5 R_E$). Finally, we determine the magnetopause stand-off distance from the *Shue et al.* (1998) model using the observed solar wind conditions ($B_Z = -5$ nT and $p = 3$ nPa) which gives $R_{MP} = 9.2 R_E$. Substituting these values into Equation 9 gives $\tau_{sh} = 250$ s.

The IMF was initially northward, and turned abruptly southward at 04:40 UT. The IMF then remained strongly southward (indicated by a clock angle that was very close to 180°) until 05:14 UT. Between 05:14 and 05:25 UT, the IMF B_Y component increased, causing a decrease in θ_{CA} , before returning to a strongly southward orientation. This rotation is very well matched by the enhancements in B_Y and decrease in α_{LM} at Cluster. (We note that the leading edge of the IMF B_Y enhancement is observed about a minute earlier than at Cluster. However, this corresponds to the observation of an FTE at Cluster, and so the magnetic field measured in the magnetosheath at this instance does not reflect the unperturbed magnetosheath magnetic field.)

The auroral electrojet AU and AL indices are known to increase in magnitude following a sharp southward turning in the IMF. *Gjerloev et al.* (2010) carried out a superposed epoch analysis of AU and AL during intervals when the IMF made an abrupt southward turn, and found that AU and AL began to increase in magnitude ~ 7 minutes and ~ 24 minutes after the IMF change respectively. In the bottom panel of Figure 3 it can be seen that the magnitudes of the AU and AL indices were initially small, but started to increase at about 04:50 UT and 05:00 UT respectively, about 10 and 20 minutes after the southward IMF turn appeared in the Wind data; the delays between the southward turning of the IMF observed in the lagged OMNI data and the responses of the auroral electrojet indices are consistent with the results of *Gjerloev et al.* (2010), giving confidence in the timing of the southward turning of the IMF observed by OMNI.

During this interval, Geotail was situated much closer to Earth, just upstream of the bow shock near the dawn terminator at $(1.0, -21, -16)_{GSM} R_E$, and observed a similar antisunward component of the solar wind velocity (470 km s^{-1}). If a lag of 110 s is applied to the Geotail magnetic field observations (to represent the data being propagated back to the bow shock and then lagged by τ_{sh}), the magnetosheath B_Y increase observed by Cluster is well matched by a similar increase at Geotail, but the southward turning of the IMF occurred at 04:57 UT (not shown) – much later than in the OMNI IMF data and after the start of the increase in AU. Since the AU increase is likely to be triggered by the change in IMF, we conclude that the OMNI observations provide a more reliable estimate of the magnetosheath magnetic field direction whilst Cluster was in the magnetosphere. At the same time, ACE was close to the L1 Lagrangian point at $(240, 37, -8)_{GSM} R_E$ and observed a similar solar wind velocity. If the IMF observed by ACE is lagged by 56 minutes (52 minutes to the bow shock and 250 s through the magnetosheath), then the correspondence between the lagged IMF and the magnetosheath magnetic field observed by Cluster is considerably poorer. Therefore, in Figures 1 and 3, we use the OMNI data, lagged as described above.

4.3 Location of reconnection site

The strongly southward IMF that is observed between 04:40 and 05:14 UT indicates that the magnetosheath magnetic field was highly likely to be strongly southward during this period. This is verified by direct measurements of the magnetosheath magnetic field after 05:05 UT. Consequently, between 04:40 UT and 05:14 UT, the magnetic shear at the magnetopause was very close to 180° . Between 05:14 and 05:25 UT, the magnetosheath magnetic field was southward but with a duskward component.

The FTE signatures observed between 04:54 and 05:25 UT were standard polarity events, indicating that they were moving northward (*Cowley*, 1982) and so the reconnection site was southward of the spacecraft throughout the interval. This is consistent with the expectation for a component reconnection site passing near the subsolar point (*Gonzalez and Mozer*, 1974). The expected orientation of the X-line can be calculated from Equation 1 of *Gonzalez and Mozer* (1974):

$$\sin \beta = \frac{B_2 - B_1 \cos \alpha}{(B_1^2 + B_2^2 - 2B_1B_2 \cos \alpha)^{\frac{1}{2}}} \quad (10)$$

where B_1 and B_2 are the magnitudes of the magnetosheath and magnetospheric magnetic fields respectively, α is the angle between the magnetosheath and magnetospheric magnetic field vectors (equivalent to α_{LM} or θ_{CA} in Figure 1) and β is the angle between the magnetospheric magnetic field (or $\hat{\mathbf{I}}$) and

the reconnection line. During the strongly southward IMF period (04:40 to 05:14 UT), $\alpha = 180^\circ$ and so $\beta = 90^\circ$; therefore we would expect a component X-line to be aligned parallel to the GSM Y axis (or $\hat{\mathbf{m}}$) and southward of the spacecraft. The lowest value of θ_{CA} observed during the B_Y enhancement is 120° ; taking this to be the lowest value of α , and taking $B_1 = 50$ nT and $B_2 = 70$ nT (from Figure 1), gives a minimum value of $\beta = 65^\circ$ between 05:14 and 05:25 UT. Therefore the largest expected angle between the X-line and $\hat{\mathbf{m}}$ is 25° . During this time, the X-line is expected to be aligned from the $[Y_{GSM} > 0, Z_{GSM} > 0]$ quadrant to the $[Y_{GSM} < 0, Z_{GSM} < 0]$ quadrant (or equivalently from $[L > 0, M < 0]$ to $[L < 0, M > 0]$), but still southward of the spacecraft.

5 Results

Now that an overview of the interval has been provided, we turn our attention to the application of the single-spacecraft techniques described in Section 2 to the FTEs observed on the 27th March. As the most noticeable differences in Figure 1 occur between the observations at Clusters 1 and 2, and these two spacecraft are the most azimuthally separated, we will apply the single-spacecraft techniques to the data from these two spacecraft. Since the the maximum separation of the spacecraft in the direction normal to the magnetopause is 1,300 km, which is much less than estimates of the typical scale size of FTE structures normal to the magnetopause (Saunders et al., 1984; Rijnbeek et al., 1984), we expect much of the difference between observations at different spacecraft to be due to differences in FTE structure along the magnetopause rather than due to being observed at different distances from the magnetopause.

The electron distribution parallel and antiparallel to the magnetic field and the full-resolution magnetic field observed by Clusters 1 and 2 are shown in Figures 4 and 5 respectively, which highlight the FTEs selected for analysis in this Section. The higher flux of electrons at energies greater than 1 keV moving antiparallel to the magnetic field whilst the spacecraft are in the magnetosheath (e.g. between 05:10 and 05:15 UT in Figure 4) indicates that the spacecraft are northward of the reconnection site, consistent with the presence of standard polarity FTE signatures. FTEs where no electron signature is observed either parallel or antiparallel to the magnetic field are ‘draping-only’ signatures, and are marked by red boxes and numbered D1-D4 on Cluster 1 and D1-D5 on Cluster 2. FTEs which did occur when an electron signature was observed are shown in purple boxes and numbered C1-C9 and C1-C7. Since we are applying single-spacecraft techniques, this numbering system is not meant to imply a correspondence between signatures at two different spacecraft; for example, signature C9 at Cluster 1 is highly likely to be caused by the passage of the same FTE as signature C7 at Cluster 2.

5.1 Minimum variance analysis

We start by applying minimum variance analysis to the simplest case – ‘draping only’ signatures. We identified four draping-only signatures observed by Cluster 1 and five observed by Cluster 2, which are highlighted by red boxes in Figures 4 and 5.

The results of the *Khrabrov and Sonnerup* (1998) analysis for the draping signatures observed by Clusters 1 and 2 are listed in Tables 2 and 3 respectively. Each table lists, from left, (1) the reference number of the FTE; (2) the start and (3) end time used for the minimum variance analysis (also indicated by the left- and right-hand edges of each red box in Figures 4 and 5); (4) the ratios of the intermediate to minimum and maximum to intermediate eigenvalues (λ_2/λ_1 and λ_1/λ_2 , top and bottom rows within each major row respectively); (5) the minimum, intermediate and maximum eigenvectors ($\hat{\mathbf{x}}_3$, $\hat{\mathbf{x}}_2$ and $\hat{\mathbf{x}}_1$ – top, middle and bottom rows of each major row respectively) and (6) the angle between each eigenvector and the magnetopause normal vector $\hat{\mathbf{n}}$ determined for that spacecraft. In each case, $\hat{\mathbf{x}}_3$ is well-determined, with a ratio $\lambda_2/\lambda_3 > 3$ in all cases, and only two events having $\lambda_2/\lambda_3 < 10$. $\hat{\mathbf{x}}_1$ and $\hat{\mathbf{x}}_2$ are less well determined (aside from being well constrained to lie within the plane perpendicular to $\hat{\mathbf{x}}_3$). The ratio λ_1/λ_2 varies between 1.5 and 2.4 at Cluster 1, and between 1.1 and 1.3 at Cluster 2. In each case, $\hat{\mathbf{x}}_3$ is within 20° of the magnetopause plane. In some cases, one of the eigenvectors is a reasonable approximation of the magnetopause normal (e.g. out of the Cluster 2 events, $\hat{\mathbf{x}}_2$ & $\hat{\mathbf{n}}$ are only 6° apart for D4 and $\hat{\mathbf{x}}_1$ & $\hat{\mathbf{n}}$ are only 8° apart for D2). However, in other cases, both eigenvectors fail to pick out the magnetopause normal. This is not surprising, since $\lambda_1 \approx \lambda_2$ in most cases.

The tables continue with: (7) the rotation angle θ_n calculated for Case 2 ($\hat{\mathbf{x}}_2 \approx \hat{\mathbf{n}}$) and Case 1 ($\hat{\mathbf{x}}_1 \approx \hat{\mathbf{n}}$) from Equations 2 and 1; (8) the unrotated axial direction ($\hat{\mathbf{x}}_3$), which assumes incompressible

flow (Farrugia et al., 1987) and the axes $\hat{\mathbf{z}}_2$ & $\hat{\mathbf{z}}_1$ for compressible flow (Case 2 and Case 1) determined by rotating $\hat{\mathbf{x}}_3$ clockwise about the eigenvector $\hat{\mathbf{x}}_2$ or $\hat{\mathbf{x}}_1$ by θ_n for the relevant case; (9) the angles between the azimuthal axis in the boundary normal frame derived for the spacecraft ($\hat{\mathbf{m}}$) and the three possible axial directions $\hat{\mathbf{x}}_3$, $\hat{\mathbf{z}}_2$ & $\hat{\mathbf{z}}_1$ and (10) a comparison between the unperturbed magnetic field \mathbf{B}_0 and the mean magnetic field within the MVA interval $\langle \mathbf{B} \rangle$. These two vectors are very similar in all cases (the maximum angular difference being 7° at Cluster 1 and 1.3° at Cluster 2, and the maximum magnitude difference being 3.5%), indicating that the assumptions made by Khrabrov and Sonnerup (1998) are valid for these FTEs.

The best estimate for each FTE axis is highlighted in bold in Tables 2 and 3. This is determined as follows:

1. If $\hat{\mathbf{x}}_1 \cdot \hat{\mathbf{n}} > 0.8$, then we take the maximum variance eigenvector to be a reasonable approximation of the magnetopause normal, and the axis $\hat{\mathbf{z}}_1$ is selected.
2. If $\hat{\mathbf{x}}_2 \cdot \hat{\mathbf{n}} > 0.8$, then we take the intermediate eigenvector to be a reasonable approximation of the normal, and $\hat{\mathbf{z}}_2$ is selected.
3. If neither condition is satisfied, then we take the unrotated minimum variance eigenvector to be the best approximation of the FTE axial direction.

These axes are plotted in Figure 6 (Cluster 1) and Figure 7 (Cluster 2); the axes are closely aligned to the $\hat{\mathbf{m}}$ axis with the exception of FTE D1 at Cluster 2. In the cases where neither $\hat{\mathbf{z}}_1$ nor $\hat{\mathbf{z}}_2$ could be selected, the rotation angle θ_n would have been small (less than 4°) for either Case 1 or Case 2. This reflects the conclusion of Walthour et al. (1993, 1994) that maximum and intermediate eigenvectors that are poorly defined with respect to each other correspond to the case when θ_n is small.

We also attempted minimum variance analysis on two of the ‘core-crossing’ FTEs (Cluster 2 FTEs C1 and C2), but obtained results which were inconsistent with the assumptions made in the modeling studies such as Xiao et al. (2004). Neither FTE exhibited a strong core magnetic field (Figure 5), and so from the results of Xiao et al. (2004) we would predict that the intermediate variance direction should identify the axial direction whether or not a strong core field were present deeper inside the FTE (and hence unobserved). The intermediate variance direction was not as well-defined as we would wish with respect to either of the other two eigenvectors ($\lambda_2/\lambda_3 = 2.5$ & 2.8 ; $\lambda_1/\lambda_2 = 4.3$ & 6.2), but the intermediate eigenvector had its strongest component in the $\hat{\mathbf{n}}$ direction. If an FTE did have an axial direction normal to the magnetopause (e.g. at the point where the flux crosses the magnetopause in the Russell and Elphic (1978) model) then the expected B_N signature would be monopolar, rather than the bipolar signature that is identified. The failure of MVA to find self-consistent axes in these cases is consistent with the conclusion by Xiao et al. (2004) that minimum variance analysis on the magnetic field is not necessarily the best means of identifying the axis of FTEs if the spacecraft does sample the flux rope itself, rather than just the draping region.

5.2 Faraday’s Law

In this section, we apply the method based on Faraday’s Law that was proposed by Sonnerup and Hasegawa (2005). This method requires that the spacecraft enters onto the flux rope itself, rather than observing only the draping region, and so we apply the method to the ‘core crossing’ FTEs C1-9 on Cluster 1 and C1-7 on Cluster 2. The start and end times used for this method (corresponding to the vertical edges of the purple boxes in Figures 4 and 5) were selected based on the electron distributions to ensure that the spacecraft was on open field lines throughout.

The method involves finding the eigenvectors for the matrix given in Equation 6, which depend upon the electric and magnetic fields observed during the FTE. We take a different approach for each of the two spacecraft, in order to compare the relative merits of using different instruments to determine the electric field. For Cluster 1, we calculate the electric field vector from the cross product of the ion velocity and the magnetic field, both of which make direct 3D measurements of the parameters they observe. However, as a whole spin of the spacecraft is required to make a complete measurement of the ion distribution (from which the velocity is determined), this restricts the analysis to spin cadence data. For Cluster 2, we use the electric field measured by the EFW experiment. This allows use of higher cadence data (the electric field is measured at 25 Hz, and we use the full resolution magnetic field), but

the disadvantage is that the out-of-plane component of the electric field is inferred from the assumption $\mathbf{E} \cdot \mathbf{B} = 0$, and is only available when the conditions detailed in Section 3 are satisfied.

The results are outlined in Tables 4 and 5. The columns of each table detail: (1) the FTE number; (2) the start and (3) stop time used for the minimum variance analysis; (4) the intermediate to minimum eigenvalue ratio of the matrix \mathbf{M}_0 ; (5) the minimum eigenvector $\hat{\mathbf{k}}$, which is the estimator of the axial direction; (6) the quantity $\mathbf{U}_0 \cdot \hat{\mathbf{k}}/|\mathbf{U}_0|$, where the velocity \mathbf{U}_0 is given by Equation 8; (7) the proper velocity of the structure \mathbf{V}_0 ; and (8) the number of data points in the time series used for MVA. Table 4 also lists (9) a parameter ρ_k which will be discussed in Section 5.3.

Unlike the results of the minimum variance analysis on the draping signatures, most of the axial directions are directed poleward (shown in Figures 8 and 9), although there are some exceptions. The two main variables that *Sonnerup and Hasegawa* (2005) proposed to indicate the accuracy of the determined axial direction were the eigenvalue ratio λ_2/λ_3 and the value of $\mathbf{U}_0 \cdot \hat{\mathbf{k}}/|\mathbf{U}_0|$ (since the velocity \mathbf{U}_0 should be perpendicular to the axial direction). Only two signatures (C5 on Cluster 1 and C2 on Cluster 2) satisfy the criteria that $|\mathbf{U}_0 \cdot \hat{\mathbf{k}}/|\mathbf{U}_0| < 0.05$ and $\lambda_2/\lambda_3 > 5$. Both are events for which the Faraday's Law method estimates an axial direction that is largely aligned with $\hat{\mathbf{l}}$.

If the axes of the ‘core crossing’ FTEs observed by Cluster 1 are calculated using the Faraday's Law method with high resolution EFW data from Cluster 1 (not shown), then the results differ from those based on the CIS and FGM data, and are more like the results from Cluster 2: FTE C9 has a similar axis to that obtained using the electric field from CIS and FGM (Figure 8) (also similar to the axis determined from signature C7 at Cluster 2, which is likely to be caused by the passage of the same flux rope), but the other axes are all directed largely along $\hat{\mathbf{l}}$.

5.3 Grad Shafranov method

Another means of checking the quality of the results in Section 5.2 is to apply the first stages of Grad Shafranov reconstruction. If the axial directions determined in Section 5.2 are good, then the total pressure transverse to the axial direction ($P_T = (p_{plasma} + B_z^2/2\mu_0)$) should be well ordered as a function of the magnitude of the magnetic field vector potential (A). The function need not be linear; we therefore calculated the Spearman's Rank correlation coefficient (ρ_k) between these two parameters, which is provided in the final column of Table 4. (Since this requires knowledge of the plasma pressure, it has only been calculated for Cluster 1.) With the exception of the shorter-duration events (with fewer than ten data points), the events where \mathbf{k} is mainly poleward give rise to relatively weak correlation coefficients (all less than 0.6) and the events where $\hat{\mathbf{k}}$ is mostly azimuthal all give rise to stronger coefficients. This suggests that the poleward axes might not be very well determined, notwithstanding the fact that other two quality parameters may be satisfied (e.g. signature C5).

The final method we used to determine the FTE axis was that proposed by *Hau and Sonnerup* (1999). First, the proper frame of the structure was calculated using de Hoffmann-Teller analysis. A trial axis was then defined by an angle θ within the $\hat{\mathbf{l}}-\hat{\mathbf{m}}$ plane. The tangential total pressure and vector potential were calculated and the Spearman's Rank correlation (ρ) between these two parameters was calculated. (Again, since this requires knowledge of the plasma pressure, this method was only applied to Cluster 1.) The axis angle θ was varied in 1° intervals between $\pm 90^\circ$, and the angle θ_{MAX} which maximized the correlation coefficient (ρ_{MAX}) was selected as the axial direction.

The results of this analysis are provided in Table 6, which lists (1-3) the interval used for the analysis (which is the same as used in Section 5.2); (4) the de Hoffmann-Teller velocity in boundary normal coordinates (\mathbf{V}_{HT}), which is the velocity of the proper frame used in the analysis; (5) the correlation (r_{HT}) between the observed electric field $-\mathbf{v} \times \mathbf{B}$ and the electric field of the proper frame $-\mathbf{V}_{HT} \times \mathbf{B}$, which indicates the quality of the de Hoffmann-Teller frame; (6) ρ_{MAX} ; (7) θ_{MAX} ; (8) the axis defined by θ_{MAX} in boundary normal coordinates, which is taken to be the axial direction of the FTE and (9) the number of data points used in the analysis. The plots of P_T against A for the optimized axial direction for each FTE are shown in Figure 10. In some cases (particularly those with the fewest data points), the correlation coefficient was equal to ρ_{MAX} over a range of angles. In these cases, the value of θ_{MAX} is obtained by calculating the mean axial direction of the values of θ which give rise to a correlation of ρ_{MAX} , as described by *Mardia and Jupp* (2000, pp. 5 & 15).

This method also produces a mixture of axial directions (plotted in Figure 11), with some being poleward and others more azimuthal. However, the events with poleward-directed axes (C1, C2, C4, C7 & C8) are either determined from relatively few data points (< 10) or have a relatively small maximum

correlation coefficient ($\rho_{MAX} < 0.8$). [In cases with relatively few data points, the correlation coefficient does not vary sensitively with axial direction.] In Figure 11, the axes which have been determined from fewer than 10 data points or which give rise to $\rho_{MAX} < 0.8$ have been plotted with dashed arrows, whereas the axes with more data points and a strong correlation coefficient are indicated by solid arrows. If these two criteria are required to be satisfied in order to be sure that the axis has been determined reliably, then the Grad Shafranov method calculates axial directions which are mainly azimuthal. This is consistent with the results in Section 5.1. Use of these two criteria suggests that the poleward-directed axes determined by the Faraday's Law method are poorly defined; the azimuthally directed axes are better determined, but are not quite the same as the directions which best order the expected relationship between the total pressure and the vector potential.

It should be noted that Cluster 1 FTEs C7, C8 and C9 (and C7 at Cluster 2) occurred during the period when the magnetosheath magnetic field rotated towards a slightly more duskward orientation (reducing α_{LM} in Figure 1). During this interval, the effect of the decreased B_M (increased B_Y) would be to rotate a subsolar component reconnection line anticlockwise in the plane of Figures 6-9 and 11 by up to 25° (see Section 4.3). The axes of FTEs C7 and C8 are rotated in such a manner in Figure 11, but by much more than the expected 25° . Since the Grad Shafranov calculation is based on relatively few data points, we cannot safely conclude that the axes are well determined in these two cases.

The angle between the magnetosheath and magnetospheric magnetic fields (α_{LM}) immediately after the passage of FTE C9 is approximately 155° ; applying Equation 10 using $\alpha = 155^\circ$ and the same values of B_1 and B_2 as in Section 4.3 results in an expected X-line orientation of $\beta = 80^\circ$ (i.e. an anticlockwise rotation of 10° in the plane of Figure 11). Therefore, although the axis determined in this section for FTE C9 is rotated slightly clockwise relative to $\hat{\mathbf{m}}$, it lies within 15° of the orientation that is expected from a structure formed by single or multiple X-line reconnection.

6 Discussion

In this paper, we have presented observations of flux transfer events during a crossing of the magnetopause by the Cluster spacecraft on 27th March 2007. *Fear et al.* (2010b) have previously discussed these FTEs in the context of the observation of some of the events by all four spacecraft, but they noted that there were also some cases where some FTEs were observed by Cluster 1 and not Cluster 2, and vice versa. Since these two spacecraft were the most azimuthally separated, and the spacecraft are all contained within 1,300 km of a plane tangential to the magnetopause, it is likely that these differences are due to the azimuthal separation of the spacecraft rather than their differing distances from the magnetopause.

In order to investigate the structure of the FTEs, we have compared three different single-spacecraft methods for determining the axial direction of FTEs. First, we applied minimum variance analysis to the signatures observed by Clusters 1 and 2 for several events where the spacecraft only observed the draping of unreconnected flux around the open field lines which make up the FTE core. Raw MVA on draped magnetic field signatures assumes that the plasma flow is incompressible (*Farrugia et al.*, 1987). Where the intermediate or maximum variance eigenvector was aligned with the magnetopause normal, a correction that removes this assumption was also calculated using the method derived by *Khrabrov and Sonnerup* (1998). This gives rise to axial directions which are mainly directed azimuthally (Tables 2 & 3 and Figures 6 & 7). For both Clusters 1 and 2, the axes become more closely aligned with $\hat{\mathbf{m}}$ as the spacecraft approach the magnetopause. Our limited attempts to apply minimum variance analysis to the magnetic field of magnetospheric FTEs with electron signatures (indicating that the spacecraft entered onto the flux rope proper) lead us to agree with *Xiao et al.* (2004) that MVA on the magnetic field may be successful on draping-only signatures, but is not necessarily the best way to determine the axis of an FTE when the open magnetic field lines are sampled by the spacecraft.

The method based on Faraday's Law (*Sonnerup and Hasegawa*, 2005) produces a mixture of axial directions regardless of the source of the electric field measurements (Tables 4 and 5 and Figures 8 and 9). The proposed quality parameters (the eigenvalue ratio and the quantity $\mathbf{U}_0 \cdot \hat{\mathbf{k}}/|\mathbf{U}_0|$) are only satisfied in two cases, both of which have axes which are directed poleward. If the quality is determined by calculating the correlation coefficient between the transverse pressure and the magnetic field vector potential (which should be well-ordered if the axial direction has been correctly determined), then the azimuthal axes appear to be better determined than the poleward-directed axes, even for events with lower eigenvalue ratios.

If the Grad Shafranov method is used to determine the axial direction directly (which requires measurements of the ion distribution) a mixture of poleward-directed and azimuthal axial directions is also obtained (Table 6 and Figure 11). However, the poleward-directed axes are all either associated with short-duration events which only allow fewer than 10 data points to be used in the analysis, or they give rise to a relatively poor correlation between the total pressure and the magnetic field vector potential. Therefore, we conclude that the poleward-directed axes for the ‘core crossing’ FTE signatures are not reliably determined.

Therefore, the most reliably-determined axes in this study are directed mainly azimuthally, which is consistent with the longer X-line models (*Lee and Fu, 1985; Southwood et al., 1988; Scholer, 1988*). It is of particular interest to examine the axial direction of FTEs which were only observed by a subset of the spacecraft, for two reasons. The first reason is that the multi-spacecraft techniques used by *Fear et al. (2010b)* to compare the azimuthal and poleward scale sizes cannot be applied to these events. Secondly, if it is possible to establish that the Cluster tetrahedron is situated at the edge of the FTE structure, then this provides a further test of the FTE model predictions. One limitation of the procedure used in this paper is that if the shear is less than 180° , a *Russell and Elphic (1978)* flux tube can ‘relax’ and adopt a more azimuthal axis [e.g. *Fear et al., 2008*], although ultimately it must adopt a magnetospheric alignment at its magnetospheric end.

Figure 12 shows the values of B_N observed by all four spacecraft between 04:54 and 04:58 UT. Three signatures are observed by Cluster 1 (D2, D3 & D4). These are preceded by three signatures observed by Clusters 3 and 4 (situated equatorward of Clusters 1 and 2), although the second and third signatures are not quite as clear as at Cluster 1. Only the first and last of these three signatures are observed at Cluster 2 (signatures D2 and D3). Since Cluster 2 and Cluster 1 were both situated in the magnetosphere, but Cluster 2 (which did not observe the FTE) was situated closer to the magnetopause, this indicates that even if a *Russell and Elphic (1978)* flux tube does have an azimuthally directed axis (if the magnetopause shear is less than 180°), then it must still adopt a magnetospheric (i.e. poleward) orientation in between these two spacecraft, as shown in Figure 13. (If the poleward turning of the flux tube occurred dawnward of Cluster, then the FTE would be observed by both Cluster 2 and Cluster 1; if it occurred significantly duskward of Cluster, then the FTE would not be observed by any of the spacecraft.) On the other hand, an FTE formed by either of the longer X-line mechanisms would have a dawn-dusk axial direction even at its edge. Since the axis of this FTE was only 13° from the $\hat{\mathbf{m}}$ direction (Table 2), we have added confidence that FTE D3, observed by Cluster 1, is inconsistent with the *Russell and Elphic (1978)* model. We note that a similar conclusion has recently been reached by *Eastwood et al. (2012)* based on the axes determined for FTEs observed on the magnetopause flank $67 R_E$ downtail. In their case, the ‘anchoring’ of one end of a *Russell and Elphic (1978)* flux tube in the polar ionosphere leads to a different prediction for the axial direction of an FTE observed far downtail compared with that expected for a longer X-line structure observed in the same region.

Signatures C9 at Cluster 1 and C7 at Cluster 2 are highly likely to be caused by the same passing structure, as a strong signature is observed at all four spacecraft between 05:22 and 05:24 UT, and there is no other discernible FTE signature for 5 minutes beforehand or afterwards (Figure 1). Three estimates have been made of the axis of this particular event: the Faraday’s Law method has been applied to the electric field calculated from the ion and magnetic field measurements at Cluster 1 and to the measured electric field observed by Cluster 2, and the Grad Shafranov method has been applied to the data from Cluster 1. The three measurements are mutually consistent, as they are all within 34° of each other, notwithstanding the fact that the eigenvalue ratio from the Faraday’s Law method using the Cluster 1 data was at the lower end of the range of eigenvalue ratios from that method (and about half of the values in the example events discussed by *Sonnerup and Hasegawa (2005)*). However, this event is the one for which the Faraday’s Law method provides the best axis as validated by the correlation between P_t and A ($|\rho_k|$ in Table 4), and it is the only event for which the method results in an azimuthally directed axis when applied to the EFW data observed by Cluster 2. It is also the largest signature, and multi-spacecraft analysis of the velocity of the structure reveals that it is the slowest-moving (*Fear et al., 2010b*). We suggest two possibilities to explain the success of the Faraday’s Law method for this event. First, it is possible that more time has passed between the formation of this FTE and its observation than in the other cases. If the structure were at a later stage in its evolution, then perhaps the criterion of the FTE being stationary in its proper frame would be better satisfied. Second, modeling results suggest that FTEs formed by multiple X-line reconnection might be larger and slower-moving than those formed by single X-line reconnection (*Ku and Sibeck, 2000*). Given the lower velocity and

larger scale of this event compared with the earlier FTEs, it is possible that it was formed by multiple X-line reconnection, and the earlier events were formed by single X-line reconnection. We would expect structures formed by multiple X-line reconnection (which are genuine flux ropes) would be more likely to satisfy the Faraday's Law method criteria than structures formed by single X-line reconnection (which are bundles of reconnected flux, but not flux ropes).

7 Conclusions

In this paper, we have presented observations of flux transfer events from a magnetopause crossing made by the four Cluster spacecraft on 27th March 2007. The separation of the spacecraft was relatively large, and despite the fact that all four spacecraft were at similar distances from the magnetopause there were differences between the structures observed at the two most azimuthally-separated spacecraft (Clusters 1 and 2). We have applied three single-spacecraft methods to determine the axial direction of the FTEs; we find that we obtain mutually consistent results from (a) application of MVA to the magnetic field observed when the spacecraft does not cross onto open magnetic field lines, and (b) a method based on Grad Shafranov reconstruction applied to data when the spacecraft does cross onto open magnetic field lines. A method based on Faraday's Law does provide consistent axial directions in some cases, but we find that the most satisfactory means of checking the results is to carry out the first stages of Grad Shafranov reconstruction. Methods (a) and (b) give rise to axes that are directed along the dawn-dusk direction, which is more consistent with longer X-line models than the *Russell and Elphic* (1978) model. We obtain an axial direction from one particular FTE which was observed at Cluster 1 and not Cluster 2, notwithstanding the fact that the latter spacecraft was nearer the magnetopause. As the Cluster tetrahedron observes the edge of the FTE and the axis is still directed dawn-dusk, this provides added confidence that the structure is more consistent with a longer X-line mechanism.

Acknowledgements

We are grateful to the Cluster FGM, EFW, CIS and PEACE PIs and instrument teams (E. A. Lucek, M. André, I. Dandouras and A. N. Fazakerley) and to the Cluster Active Archive (<http://caa.estec.esa.int/caa/>) for providing the data used in this study. OMNI data were obtained from the GSFC/SPDF OMNIWeb interface at <http://omniweb.gsfc.nasa.gov>, and based upon Wind MFI and SWE observations courtesy of R. Lepping and K. Ogilvie. Work at Leicester was supported by STFC rolling grant ST/H002480/1. KO is supported by the Research Council of Norway. RCF would like to thank L. Trenchi and H. Hasegawa for several useful conversations about the techniques used in this paper, A. Pedersen for his advice on the use of EFW data and the referees for thought-provoking comments.

References

- Balogh, A., et al. (2001), The Cluster Magnetic Field Investigation: overview of in-flight performance and initial results, *Ann. Geophys.*, *19*, 1207–1217.
- Cooling, B. M. A., C. J. Owen, and S. J. Schwartz (2001), Role of the magnetosheath flow in determining the motion of open flux tubes, *J. Geophys. Res.*, *106*(A9), 18,763–18,775, doi:10.1029/2000JA000455.
- Cowley, S. W. H. (1982), The Causes of Convection in the Earth's Magnetosphere: A Review of Developments During the IMS, *Rev. Geophys. Space Phys.*, *20*(3), 531–565, doi:10.1029/RG020i003p00531.
- Cowley, S. W. H., and C. J. Owen (1989), A simple illustrative model of open flux tube motion over the dayside magnetopause, *Planet. Space Sci.*, *37*, 1461–1475, doi:10.1016/0032-0633(89)90116-5.
- Dandouras, I., A. Barthe, E. Penou, S. Brunato, H. Rème, L. M. Kistler, M. B. Bavassano-Cattaneo, and A. Blagau (2010), Cluster Ion Spectrometry (CIS) Data in the Cluster Active Archive (CAA), in *The Cluster Active Archive - Studying the Earth's Space Plasma Environment*, edited by H. Laakso, M. Taylor, and P. Escoubet, pp. 51–72, Springer Netherlands, Dordrecht, doi:10.1007/978-90-481-3499-1_3.

- De Hoffmann, F., and E. Teller (1950), Magneto-Hydrodynamic Shocks, *Phys. Rev.*, *80*(4), 692–703, doi:10.1103/PhysRev.80.692.
- Dorelli, J. C., and A. Bhattacharjee (2009), On the generation and topology of flux transfer events, *J. Geophys. Res.*, *114*, A06213, doi:10.1029/2008JA013410.
- Eastwood, J. P., T. D. Phan, R. C. Fear, D. G. Sibeck, V. Angelopoulos, M. Øieroset, and M. A. Shay (2012), Survival of flux transfer event (FTE) flux ropes far along the tail magnetopause, *J. Geophys. Res.*, in press, doi:10.1029/2012JA017722.
- Elphic, R. C., and C. T. Russell (1983), Magnetic Flux Ropes in the Venus Ionosphere: Observations and Models, *J. Geophys. Res.*, *88*(A1), 58–72, doi:10.1029/JA088iA01p00058.
- Elphic, R. C., C. T. Russell, J. A. Slavin, and L. H. Brace (1980), Observations of the Dayside Ionopause and Ionosphere of Venus, *J. Geophys. Res.*, *85*(A13), 7679–7696, doi:10.1029/JA085iA13p07679.
- Farris, M. H., and C. T. Russell (1994), Determining the Standoff Distance of the Bow Shock: Mach Number Dependence and Use of Models, *J. Geophys. Res.*, *99*(A9), 17,681–17,689, doi:10.1029/94JA01020.
- Farrugia, C. J., R. C. Elphic, D. J. Southwood, and S. W. H. Cowley (1987), Field and flow perturbations outside the reconnected field line region in flux transfer events: Theory, *Planet. Space Sci.*, *35*(2), 227–240, doi:10.1016/0032-0633(87)90091-2.
- Fazakerley, A. N., A. D. Lahiff, R. J. Wilson, I. Rozum, C. Anekallu, M. West, and H. Bacai (2010), PEACE Data in the Cluster Active Archive, in *The Cluster Active Archive - Studying the Earth's Space Plasma Environment*, edited by H. Laakso, M. Taylor, and P. Escoubet, pp. 129–144, Springer Netherlands, Dordrecht, doi:10.1007/978-90-481-3499-1_8.
- Fear, R. C., et al. (2007), Motion of flux transfer events: a test of the Cooling model, *Ann. Geophys.*, *25*, 1669–1690, doi:10.5194/angeo-25-1669-2007.
- Fear, R. C., S. E. Milan, A. N. Fazakerley, E. A. Lucek, S. W. H. Cowley, and I. Dandouras (2008), The azimuthal extent of three flux transfer events, *Ann. Geophys.*, *26*, 2353–2369, doi:10.5194/angeo-26-2353-2008.
- Fear, R. C., S. E. Milan, J. Raeder, and D. G. Sibeck (2010a), Asymmetry in the bipolar signatures of flux transfer events, *J. Geophys. Res.*, *115*, A11217, doi:10.1029/2010JA015363.
- Fear, R. C., S. E. Milan, E. A. Lucek, S. W. H. Cowley, and A. N. Fazakerley (2010b), Mixed Azimuthal Scales of Flux Transfer Events, in *The Cluster Active Archive - Studying the Earth's Space Plasma Environment*, edited by H. Laakso, M. Taylor, and C. P. Escoubet, *Astrophys. Space Sci. Proc.*, pp. 389–398, Springer Netherlands, Dordrecht, doi:10.1007/978-90-481-3499-1_27.
- Fear, R. C., M. Palmroth, and S. E. Milan (2012), Seasonal and clock angle control of the location of flux transfer event signatures at the magnetopause, *J. Geophys. Res.*, *117*, A04202, doi:10.1029/2011JA017235.
- Gjerloev, J. W., R. A. Hoffman, S. Ohtani, J. Weygand, and R. Barnes (2010), Response of the auroral electrojet indices to abrupt southward IMF turnings, *Ann. Geophys.*, *28*, 1167–1182, doi:10.5194/angeo-28-1167-2010.
- Gloag, J. M., E. A. Lucek, L.-N. Alconcel, A. Balogh, P. Brown, C. M. Carr, C. N. Dunford, T. Oddy, and J. Soucek (2010), FGM Data Products in the CAA, in *The Cluster Active Archive - Studying the Earth's Space Plasma Environment*, edited by H. Laakso, M. Taylor, and P. Escoubet, pp. 109–128, Springer Netherlands, Dordrecht, doi:10.1007/978-90-481-3499-1_7.
- Gonzalez, W. D., and F. S. Mozer (1974), A Quantitative Model for the Potential Resulting from Reconnection with an Arbitrary Interplanetary Magnetic Field, *J. Geophys. Res.*, *79*(28), 4186–4194, doi:10.1029/JA079i028p04186.
- Gustafsson, G., et al. (2001), First results of electric field and density observations by Cluster EFW based on initial months of operation, *Ann. Geophys.*, *19*, 1219–1240, doi:10.5194/angeo-19-1219-2001.

- Hasegawa, H., B. U. Ö. Sonnerup, B. Klecker, G. Paschmann, M. W. Dunlop, and H. Rème (2005), Optimal reconstruction of magnetopause structures from Cluster data, *Ann. Geophys.*, *23*, 973–982.
- Hasegawa, H., B. U. Ö. Sonnerup, C. J. Owen, B. Klecker, G. Paschmann, A. Balogh, and H. Rème (2006), The structure of flux transfer events recovered from Cluster data, *Ann. Geophys.*, *24*, 603–618.
- Hasegawa, H., et al. (2010), Evidence for a flux transfer event generated by multiple X-line reconnection at the magnetopause, *Geophys. Res. Lett.*, *37*, L16101, doi:10.1029/2010GL044219.
- Hau, L.-N., and B. U. Ö. Sonnerup (1999), Two-dimensional coherent structures in the magnetopause: Recovery of static equilibria from single-spacecraft data, *J. Geophys. Res.*, *104*(A4), 6899–6917, doi:10.1029/1999JA900002.
- Hu, Q., and B. U. Ö. Sonnerup (2003), Reconstruction of two-dimensional structures in the magnetopause: Method improvements, *J. Geophys. Res.*, *108*(A1), 1011, doi:10.1029/2002JA009323.
- Johnstone, A. D., et al. (1997), PEACE: A plasma electron and current experiment, *Space Sci. Rev.*, *79*, 351–398, doi:10.1023/A:1004938001388.
- Khan, H., and S. W. H. Cowley (1999), Observations of the response time of high-latitude ionospheric convection to variations in the interplanetary magnetic field using EISCAT and IMP-8 data, *Ann. Geophys.*, *17*(10), 1306–1335, doi:10.1007/s00585-999-1306-8.
- Khotyaintsev, Y., P.-A. Lindqvist, A. Eriksson, and M. André (2010), The EFW Data in the CAA, in *The Cluster Active Archive - Studying the Earth's Space Plasma Environment*, edited by H. Laakso, M. Taylor, and P. Escoubet, pp. 97–108, Springer Netherlands, Dordrecht, doi:10.1007/978-90-481-3499-1_6.
- Khrabrov, A. V., and B. U. Ö. Sonnerup (1998), Magnetic variance analysis for small-amplitude waves and flux transfer events on a current sheet, *J. Geophys. Res.*, *103*(A6), 11,907–11,918, doi:10.1029/98JA00615.
- King, J. H., and N. E. Papitashvili (2005), Solar wind spatial scales in and comparisons of hourly Wind and ACE plasma and magnetic field data, *J. Geophys. Res.*, *110*, A02104, doi:10.1029/2004JA010649.
- Korotova, G. I., D. G. Sibeck, and T. Rosenberg (2008), Seasonal dependence of Interball flux transfer events, *Geophys. Res. Lett.*, *35*, L05106, doi:10.1029/2008GL033254.
- Ku, H. C., and D. G. Sibeck (1997), Internal structure of flux transfer events produced by the onset of merging at a single X line, *J. Geophys. Res.*, *102*(A2), 2243–2260, doi:10.1029/96JA03162.
- Ku, H. C., and D. G. Sibeck (1998a), The effect of magnetosheath plasma flow on flux transfer events produced by the onset of merging at a single X line, *J. Geophys. Res.*, *103*(A4), 6693–6702, doi:10.1029/97JA03688.
- Ku, H. C., and D. G. Sibeck (1998b), Flux transfer events produced by bursty merging at a single X line, *J. Geophys. Res.*, *103*(A7), 14,965–14,978, doi:10.1029/98JA01171.
- Ku, H. C., and D. G. Sibeck (2000), Flux transfer events produced by the onset of merging at multiple X lines, *J. Geophys. Res.*, *105*(A2), 2657–2675, doi:10.1029/1999JA900431.
- Laitinen, T. V., Y. V. Khotyaintsev, M. André, A. Vaivads, and H. Rème (2010), Local influence of magnetosheath plasma beta fluctuations on magnetopause reconnection, *Ann. Geophys.*, *28*, 1053–1063, doi:10.5194/angeo-28-1053-2010.
- Lee, L. C., and Z. F. Fu (1985), A theory of magnetic flux transfer at the Earth's magnetopause, *Geophys. Res. Lett.*, *12*(2), 105–108, doi:10.1029/GL012i002p00105.
- Lepping, R. P., et al. (1995), The WIND magnetic field investigation, *Space Sci. Rev.*, *71*, 207–229, doi:10.1007/BF00751330.
- Lockwood, M., and M. A. Hapgood (1998), On the cause of a magnetospheric flux transfer event, *J. Geophys. Res.*, *103*(A11), 26,453–26,478, doi:10.1029/98JA02244.

- Marchaudon, A., J.-C. Cerisier, J.-M. Bosqued, M. W. Dunlop, J. A. Wild, P. M. E. Décréau, M. Förster, D. Fontaine, and H. Laakso (2004), Transient plasma injections in the dayside magnetosphere: one-to-one correlated observations by Cluster and SuperDARN, *Ann. Geophys.*, *22*, 141–158.
- Mardia, K. V., and P. E. Jupp (2000), *Directional Statistics*, Wiley, Chichester.
- Milan, S. E., M. Lester, S. W. H. Cowley, and M. Brittnacher (2000), Convection and auroral response to a southward turning of the IMF: Polar UVI, CUTLASS, and IMAGE signatures of transient magnetic flux transfer at the magnetopause, *J. Geophys. Res.*, *105*(A7), 15,741–15,755, doi:10.1029/2000JA900022.
- Øieroset, M., et al. (2011), Direct Evidence for a Three-Dimensional Magnetic Flux Rope Flanked by Two Active Magnetic Reconnection X Lines at Earth’s Magnetopause, *Phys. Rev. Lett.*, *107*, 165007, doi:10.1103/PhysRevLett.107.165007.
- Ogilvie, K. W., et al. (1995), SWE, a comprehensive plasma instrument for the WIND spacecraft, *Space Sci. Rev.*, *71*, 55–77, doi:10.1007/BF00751326.
- Oksavik, K., T. A. Fritz, Q.-G. Zong, F. Søråas, and B. Wilken (2002), Three-dimensional energetic ion sounding of the magnetopause using Cluster/RAPID, *Geophys. Res. Lett.*, *29*(9), 1347, doi:10.1029/2001GL014265.
- Oksavik, K., J. Moen, and H. C. Carlson (2004), High-resolution observations of the small-scale flow pattern associated with a poleward moving auroral form in the cusp, *Geophys. Res. Lett.*, *31*, L11807, doi:10.1029/2004GL019838.
- Oksavik, K., J. Moen, H. C. Carlson, R. A. Greenwald, S. E. Milan, M. Lester, W. F. Denig, and R. J. Barnes (2005), Multi-instrument mapping of the small-scale flow dynamics related to a cusp auroral transient, *Ann. Geophys.*, *23*(7), 2657–2670, doi:10.5194/angeo-23-2657-2005.
- Raeder, J. (2006), Flux Transfer Events: 1. Generation mechanism for strong southward IMF, *Ann. Geophys.*, *24*(1), 381–392.
- Rème, H., et al. (2001), First multispacecraft ion measurements in and near the Earth’s magnetosphere with the identical Cluster ion spectrometry (CIS) experiment, *Ann. Geophys.*, *19*, 1303–1354.
- Rijnbeek, R. P., S. W. H. Cowley, D. J. Southwood, and C. T. Russell (1984), A survey of dayside transfer events observed by ISEE 1 and 2 magnetometers, *J. Geophys. Res.*, *89*(A2), 786–800, doi:10.1029/JA089iA02p00786.
- Robert, P., et al. (2006), Study of a flux transfer event with Cluster spacecraft, in *Proc. of the Cluster and Double Star Symposium - 5th Anniversary of Cluster in Space*, vol. 2005, ESA.
- Russell, C. T., and R. C. Elphic (1978), Initial ISEE magnetometer results: magnetopause observations, *Space Sci. Rev.*, *22*(6), 681–715, doi:10.1007/BF00212619.
- Russell, C. T., and R. C. Elphic (1979), ISEE observations of flux transfer events at the dayside magnetopause, *Geophys. Res. Lett.*, *6*(1), 33–36, doi:10.1029/GL006i001p00033.
- Saunders, M. A., C. T. Russell, and N. Sckopke (1984), Flux transfer events: Scale size and interior structure, *Geophys. Res. Lett.*, *11*(2), 131–134, doi:10.1029/GL011i002p00131.
- Scholer, M. (1988), Magnetic flux transfer at the magnetopause based on single X line bursty reconnection, *Geophys. Res. Lett.*, *15*(4), 291–294, doi:10.1029/GL015i004p00291.
- Scholer, M. (1995), Models of Flux Transfer Events, in *Physics of the magnetopause*, edited by P. Song, B. U. Ö. Sonnerup, and M. F. Thomsen, Geophysical Monograph, pp. 235–245, American Geophysical Union, Washington D. C.
- Shue, J.-H., et al. (1998), Magnetopause location under extreme solar wind conditions, *J. Geophys. Res.*, *103*(A8), 17,691–17,700, doi:10.1029/98JA01103.

- Sibeck, D. G., G. L. Siscoe, J. A. Slavin, E. J. Smith, S. J. Bame, and F. L. Scarf (1984), Magnetotail flux ropes, *Geophys. Res. Lett.*, *11*(10), 1090–1093, doi:10.1029/GL011i010p01090.
- Slavin, J. A., et al. (1989), CDAW 8 Observations of Plasmoid Signatures in the Geomagnetic Tail: An Assessment, *J. Geophys. Res.*, *94*(A11), 15,153–15,175, doi:10.1029/JA094iA11p15153.
- Sonnerup, B. U. Ö. (1988), Experimental tests of FTE theories, *Adv. Space Res.*, *8*, 263–272, doi:10.1016/0273-1177(88)90140-8.
- Sonnerup, B. U. Ö., and L. J. Cahill (1967), Magnetopause Structure and Attitude from Explorer 12 Observations, *J. Geophys. Res.*, *72*, 171–183, doi:10.1029/JZ072i001p00171.
- Sonnerup, B. U. Ö., and H. Hasegawa (2005), Orientation and motion of two-dimensional structures in a space plasma, *J. Geophys. Res.*, *110*, A06208, doi:10.1029/2004JA010853.
- Sonnerup, B. U. Ö., and M. Scheible (1998), Minimum and Maximum Variance Analysis, in *Analysis Methods for Multi-Spacecraft Data*, edited by G. Paschmann and P. W. Daly, pp. 185–220, ISSI, Bern.
- Sonnerup, B. U. Ö., H. Hasegawa, and G. Paschmann (2004), Anatomy of a flux transfer event seen by Cluster, *Geophys. Res. Lett.*, *31*, L11803, doi:10.1029/2004GL020134.
- Sonnerup, B. U. Ö., H. Hasegawa, W.-L. Teh, and L.-N. Hau (2006), Grad-Shafranov reconstruction: An overview, *J. Geophys. Res.*, *111*, A09204, doi:10.1029/2006JA011717.
- Southwood, D. J., C. J. Farrugia, and M. A. Saunders (1988), What are flux transfer events?, *Planet. Space Sci.*, *36*(5), 503–508, doi:10.1016/0032-0633(88)90109-2.
- Trenchi, L., M. F. Marcucci, H. Rème, C. M. Carr, and J. B. Cao (2011), TC-1 observations of a flux rope: Generation by multiple X line reconnection, *J. Geophys. Res.*, *116*, A05202, doi:10.1029/2010JA015986.
- Walthour, D. W., B. U. Ö. Sonnerup, G. Paschmann, H. Lühr, D. Klumpar, and T. Potemra (1993), Remote Sensing of Two-Dimensional Magnetopause Structures, *J. Geophys. Res.*, *98*(A2), 1489–1504, doi:10.1029/92JA02206.
- Walthour, D. W., B. U. Ö. Sonnerup, R. C. Elphic, and C. T. Russell (1994), Double Vision: Remote Sensing of a Flux Transfer Event with ISEE 1 and 2, *J. Geophys. Res.*, *99*(A5), 8555–8563, doi:10.1029/93JA03440.
- Xiao, C. J., Z. Y. Pu, Z. W. Ma, S. Y. Fu, Z. Y. Huang, and Q. G. Zong (2004), Inferring of flux rope orientation with the minimum variance analysis technique, *J. Geophys. Res.*, *109*, A11218, doi:10.1029/2004JA010594.
- Zong, Q.-G., et al. (1997), Geotail observations of energetic ion species and magnetic field in plasmoid-like structures in the course of an isolated substorm event, *J. Geophys. Res.*, *102*(A6), 11,409–11,428, doi:10.1029/97JA00076.

Spacecraft	MVA interval	$\lambda_{int}/\lambda_{min}$	$\hat{\mathbf{n}}_{GSE}$	$\hat{\mathbf{m}}_{GSE}$	$\hat{\mathbf{i}}_{GSE}$
Cluster 1	05:06–05:10 UT	2.14	(0.916, 0.149, 0.372)	(-0.007, -0.923, 0.386)	(-0.401, 0.356, 0.844)
Cluster 2	05:03–05:10 UT	2.63	(0.880, -0.128, -0.457)	(-0.302, -0.894, 0.331)	(-0.366, 0.429, 0.826)
Cluster 3	05:03–05:10 UT	2.62	(0.958, -0.014, 0.285)	(-0.123, -0.922, 0.368)	(-0.257, 0.388, 0.885)
Cluster 4	05:06–05:10 UT	4.42	(0.925, -0.072, 0.373)	(-0.213, -0.912, 0.351)	(-0.314, 0.404, 0.859)

Table 1: Boundary normal coordinates

FTE	MVA Start (UT)	MVA Stop (UT)	λ_2/λ_3 λ_1/λ_2	Min eigenvector Int eigenvector Max eigenvector \hat{x}_1 \hat{x}_2 \hat{x}_3	Angle to \hat{n}	θ_N (Case 2) (Case 1)	MVA axis \hat{x}_3 Case 2 axis \hat{z}_2 Case 1 axis \hat{z}_1	Angle to \hat{m}	$ \mathbf{B}_0 $ $ \langle \mathbf{B} \rangle $ Difference
D1	04:50:00	04:53:00	3.4 2.4	(-0.010, 0.970, 0.242) (0.987, 0.048, -0.153) (0.160, -0.238, 0.958)	76° 99° 17°	- -3° -0.3°	(-0.015, 0.970, 0.242) (-0.001, 0.955, -0.295) (-0.015, 0.970, 0.243)	14° 17° 14°	74.3 nT 71.8 nT 7°
D2	04:54:00	04:54:15	5.7 1.5	(0.028, 0.942, -0.335) (0.639, 0.241, 0.730) (-0.768, 0.234, 0.596)	110° 43° 53°	- 0.5° -0.4°	(0.028, 0.942, -0.335) (0.035, 0.940, -0.340) (0.024, 0.940, -0.340)	20° 20° 20°	74.3 nT 72.6 nT 5°
D3	04:55:15	04:56:30	13.3 1.8	(-0.158, 0.986, -0.046) (0.796, 0.155, 0.585) (-0.584, -0.055, 0.810)	93° 54° 36°	- -14° 5°	(-0.158, 0.986, -0.046) (-0.291, 0.945, 0.146) (-0.089, 0.996, 0.004)	9° 19° 5°	74.3 nT 73.5 nT 4°
D4	04:56:30	04:57:30	66.0 1.8	(0.306, 0.922, -0.239) (0.784, -0.386, -0.486) (0.540, 0.039, 0.841)	104° 119° 33°	- -22° -10°	(0.306, 0.922, -0.239) (0.489, 0.867, 0.099) (0.165, 0.975, -0.151)	23° 30° 13°	74.3 nT 75.2 nT 5°

Table 2: Results of *Khrabrov and Somnerup* (1998) analysis on draped FTE signatures D1–4 observed by Cluster 1. All vectors are provided in the boundary normal coordinate system for Cluster 1.

FTE	MVA Start (UT)	MVA Stop (UT)	λ_2/λ_3 λ_1/λ_2	Min eigenvector \hat{x}_3 Int eigenvector \hat{x}_2 Max eigenvector \hat{x}_1	Angle to \hat{n}	θ_N (Case 2) (Case 1)	MVA axis \hat{x}_3 Case 2 axis \hat{z}_2 Case 1 axis \hat{z}_1	Angle to \hat{m}	$ \mathbf{B}_0 $ $ \langle \mathbf{B} \rangle $ Difference
D1	04:52:30	04:54:30	10.4 1.1	(-0.464, 0.857, 0.224) (0.656, 0.502, -0.563) (0.595, 0.114, 0.796)	77° 125° 37°	- 3.7° 2.8°	(-0.464, 0.857, 0.224) (-0.501, 0.848, 0.172) (-0.432, 0.880, 0.197)	31° 32° 28°	72.6 nT 72.4 nT 0.4°
D2	04:54:30	04:55:30	38.6 1.3	(-0.277, 0.958, 0.075) (0.952, 0.284, -0.117) (0.133, -0.039, 0.990)	86° 97° 8°	- 47° 4°	(-0.277, 0.958, 0.075) (-0.286, 0.682, -0.673) (-0.210, 0.976, 0.067)	17° 47° 13°	72.6 nT 71.6 nT 0.8°
D3	04:56:00	04:57:45	17.9 1.3	(-0.128, 0.982, -0.140) (0.750, 0.188, 0.634) (-0.648, 0.024, 0.761)	98° 51° 41°	- -3° 2°	(-0.128, 0.982, -0.140) (-0.162, 0.982, -0.099) (-0.099, 0.988, -0.115)	11° 11° 9°	72.6 nT 73.1 nT 0.4°
D4	04:59:45	05:00:20	21.8 1.1	(-0.124, 0.992, -0.025) (0.088, 0.036, 0.995) (-0.988, -0.121, 0.092)	91° 6° 85°	- -0.9° 19°	(-0.124, 0.992, -0.025) (-0.139, 0.990, -0.024) (-0.089, 0.950, 0.298)	7° 8° 18°	72.6 nT 73.6 nT 1.2°
D5	05:02:45	05:03:30	16.7 1.1	(-0.101, 0.995, -0.011) (0.818, 0.077, -0.570) (0.566, 0.067, 0.821)	91° 125° 35°	- 0.5° 0.3°	(-0.101, 0.995, -0.011) (-0.106, 0.994, -0.019) (-0.096, 0.995, -0.014)	6° 6° 6°	72.6 nT 72.4 nT 1.3°

Table 3: Results of *Kharabov and Somnerup* (1998) analysis on draped FTE signatures D1-5 observed by Cluster 2. All vectors are provided in the boundary normal coordinate system for Cluster 2.

FTE	MVA Start (UT)	MVA Stop (UT)	λ_2/λ_3	Min eigenvector $\hat{\mathbf{k}}$	$\frac{\mathbf{U}_0 \cdot \hat{\mathbf{k}}}{ \mathbf{U}_0 }$	\mathbf{V}_0 (km s ⁻¹)	No. pts.	$ \rho_k $
C1	05:02:37	05:02:55	6.6	(0.584, 0.701, 0.408)	0.3	(420, -96, -434)	5	0.90
C2	05:04:47	05:05:11	2.0	(0.997, -0.048, 0.058)	0.8	(10, 194, -16)	5	1.00
C3	05:07:11	05:07:53	4.0	(0.985, 0.149, 0.081)	0.08	(12, -71, -12)	11	0.38
C4	05:08:10	05:08:53	4.0	(0.906, 0.213, -0.365)	-0.1	(24, 4, 62)	10	0.58
C5	05:08:57	05:09:43	19.3	(0.981, 0.191, 0.012)	0.002	(51, -28, 2)	11	0.26
C6	05:09:49	05:10:52	2.8	(0.009, 0.997, -0.074)	0.2	(159, 0, 12)	16	0.86
C7	05:14:02	05:14:29	1.1	(0.620, -0.772, 0.139)	-0.04	(117, 94, -2)	7	0.68
C8	05:16:15	05:16:32	17.3	(0.431, 0.613, 0.663)	-0.4	(229, -65, 89)	5	0.70
C9	05:22:45	05:23:59	2.8	(0.593, 0.805, 0.018)	0.01	(85, -62, -18)	18	0.92

Table 4: Results of *Sonnerup and Hasegawa* (2005) analysis on ‘core crossing’ FTE signatures C1-9 observed by Cluster 1. All vectors are provided in the boundary normal coordinate system for Cluster 1.

FTE	MVA Start (UT)	MVA Stop (UT)	λ_2/λ_3	Min eigenvector $\hat{\mathbf{k}}$	$\frac{\mathbf{U}_0 \cdot \hat{\mathbf{k}}}{ \mathbf{U}_0 }$	\mathbf{V}_0 (km s ⁻¹)	No. pts.
C1	04:59:00	04:59:20	4.6	(0.984, 0.178, -0.025)	0.2	(-5, 29, -3)	444
C2	05:01:55	05:02:11	5.2	(0.989, 0.146, -0.025)	0.02	(-8, 50, 17)	359
C3	05:03:38	05:03:57	25.5	(0.998, -0.022, -0.054)	-0.5	(3, 110, 3)	426
C4	05:08:20	05:08:36	16.2	(0.949, 0.316, 0.014)	0.4	(6, -18, -5)	358
C5	05:10:36	05:11:34	4.9	(0.981, 0.155, -0.117)	-0.3	(7, -22, 27)	1296
C6	05:13:12	05:13:37	2.6	(0.771, -0.331, 0.544)	-0.2	(123, 88, -121)	560
C7	05:23:06	05:23:54	22.6	(0.350, 0.928, 0.126)	-0.1	(134, -46, -30)	1076

Table 5: Results of *Sonnerup and Hasegawa* (2005) analysis on ‘core crossing’ FTE signatures C1-7 observed by Cluster 2. All vectors are provided in the boundary normal coordinate system for Cluster 2.

FTE	Start (UT)	Stop (UT)	\mathbf{V}_{HT} (km s ⁻¹)	r_{HT}	ρ_{MAX}	θ_{MAX}	Axis	No. pts.
C1	05:02:37	05:02:55	(95.0, -30.7, 3.5)	0.935	1.00	11°	(0.980, 0.191, 0.000)	5
C2	05:04:47	05:05:11	(243.6, 55.5, 1.7)	0.812	1.00	-4°	(0.999, -0.070, 0.000)	5
C3	05:07:11	05:07:53	(359.4, 47.9, 23.2)	0.947	0.97	80°	(0.174, 0.985, 0.000)	11
C4	05:08:10	05:08:53	(215.4, -54.6, 37.6)	0.954	0.66	12°	(0.978, 0.208, 0.000)	10
C5	05:08:57	05:09:43	(154.1, 28.5, 4.4)	0.946	0.82	66°	(0.407, 0.914, 0.000)	11
C6	05:09:49	05:10:52	(183.9, 5.4, 1.1)	0.966	0.89	77°	(0.225, 0.974, 0.000)	16
C7	05:14:02	05:14:29	(183.2, -10.8, 2.5)	0.984	0.68	-46°	(0.695, -0.719, 0.000)	7
C8	05:16:15	05:16:32	(206.2, -24.2, -4.6)	0.996	1.00	-23°	(0.921, -0.391, 0.000)	5
C9	05:22:45	05:23:59	(198.6, 80.0, -3.5)	0.967	0.97	87°	(0.052, 0.999, 0.000)	18

Table 6: Results of the Grad Shafranov method on ‘core crossing’ FTE signatures C1-9 observed by Cluster 1. All vectors are given in boundary normal coordinates. In cases where more than one value of θ results in a correlation coefficient equal to ρ_{MAX} , θ_{MAX} is the directional mean of all such values of θ .

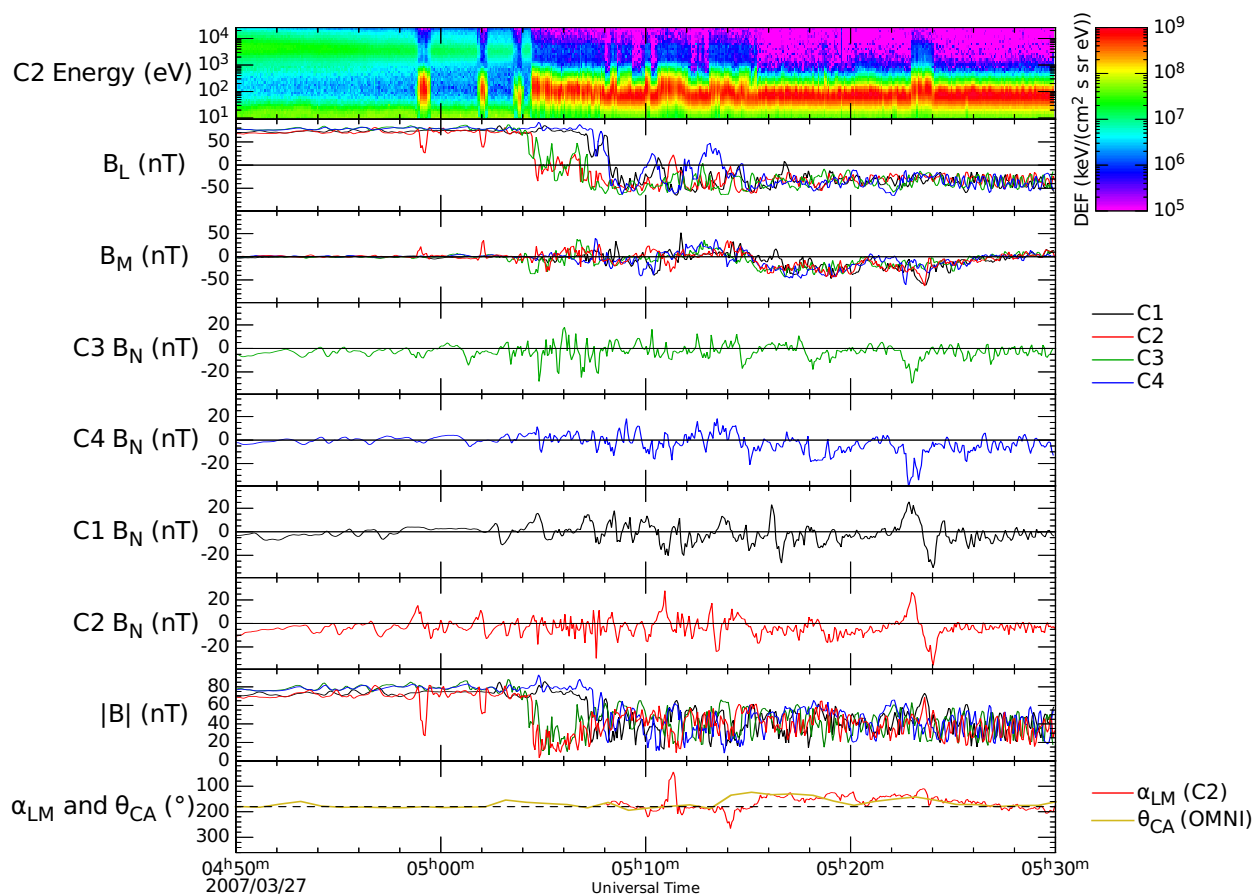


Figure 1: An overview of the interval. From top: the electron distribution observed by Cluster 2 and the B_L , B_M and B_N components & magnetic field magnitude observed by all four spacecraft. The bottom panel shows the OMNI IMF clock angle with an additional lag of 250 s to account for the propagation of the IMF through the magnetosheath to the magnetopause, and the angle made in the $\hat{\mathbf{l}} - \hat{\mathbf{m}}$ plane by the magnetic field observed by Cluster 2 (from 05:08 UT onwards).

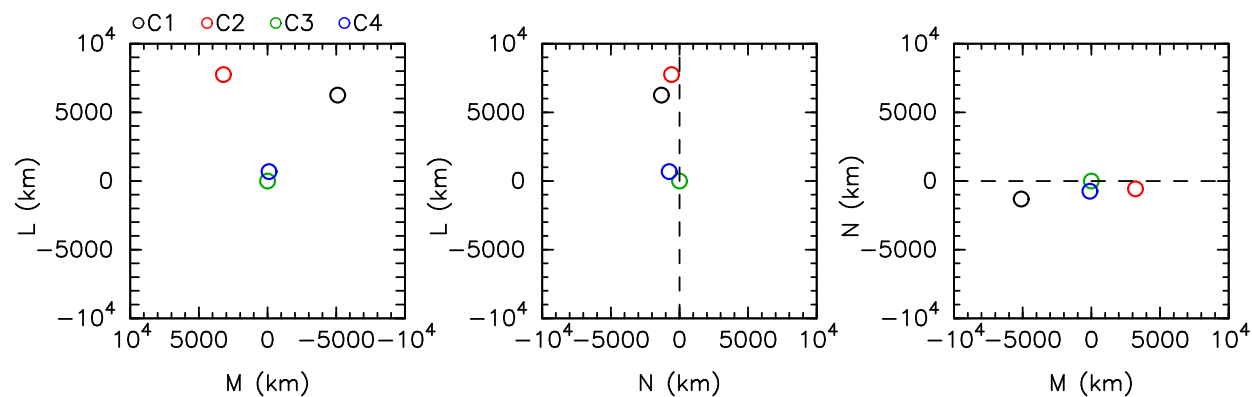


Figure 2: The orientation of the spacecraft relative to Cluster 3 in the boundary normal coordinate system for Cluster 3.

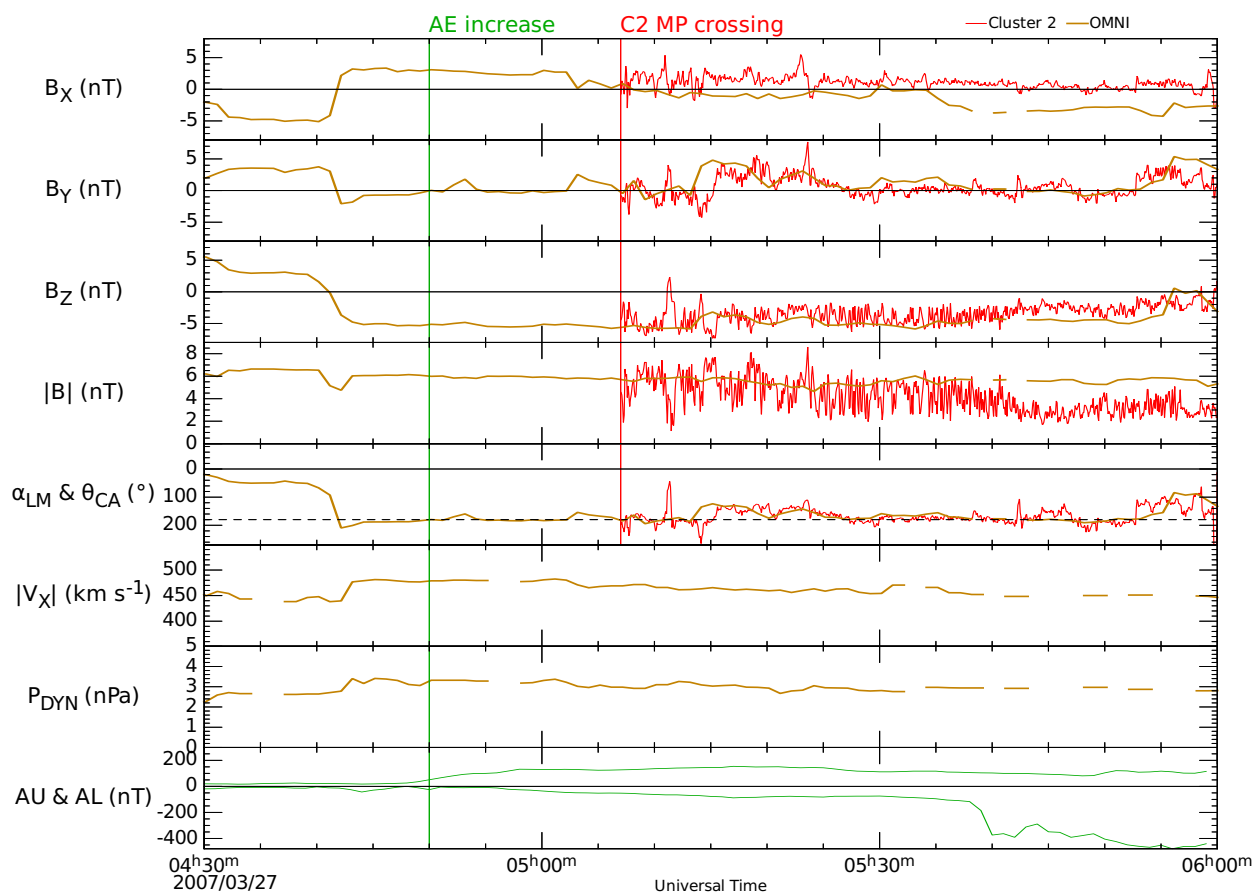


Figure 3: The lagged solar wind conditions, propagated to the bow shock by OMNI and then lagged by a further 250 s to account for the expected transport time of plasma through the magnetosheath to the magnetopause. From top: the GSM components and magnitude of the IMF and the magnetosheath magnetic field observed by Cluster 2 (divided by 8), the IMF clock angle (θ_{CA}) and the angle made by the magnetosheath magnetic field tangential to the magnetopause plane (α_{LM} , which is defined in the same sense as θ_{CA}), the antisunward component of the solar wind speed, the solar wind dynamic pressure and the auroral electrojet AU and AL indices.

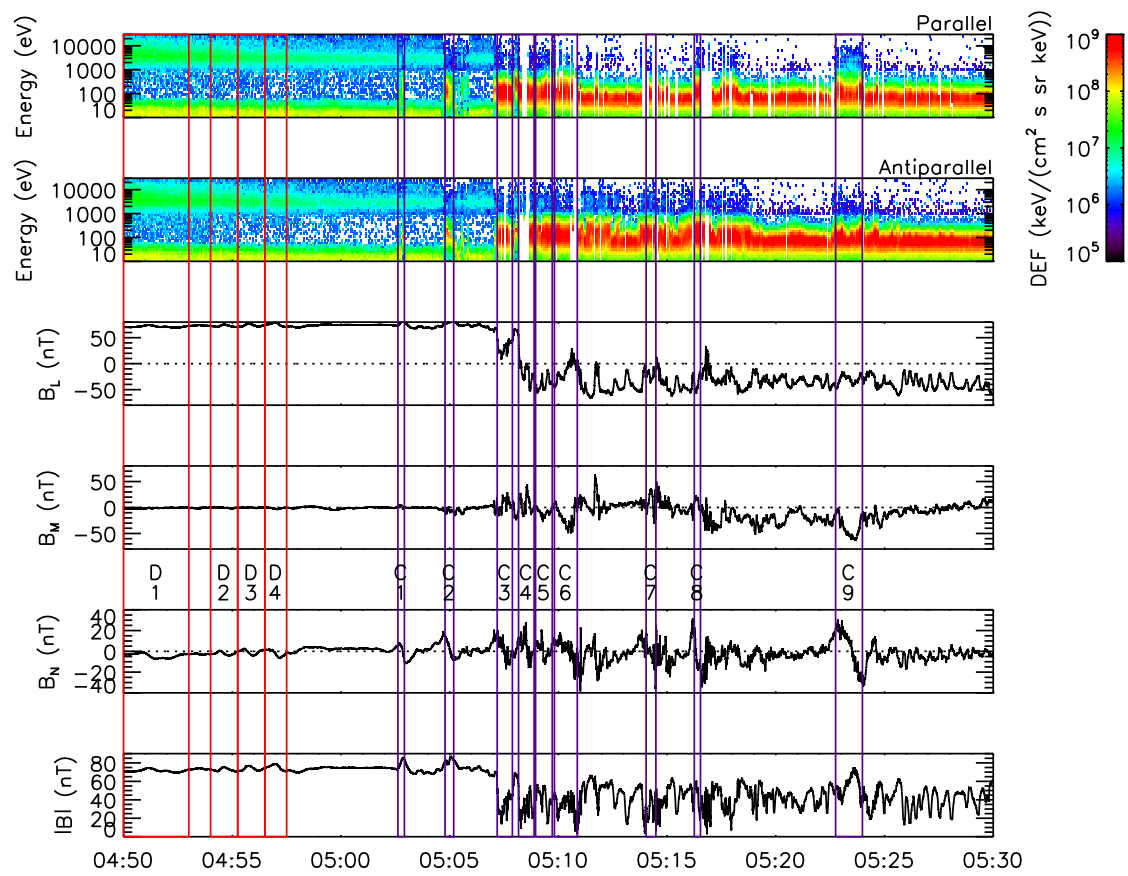


Figure 4: The FTEs observed by Cluster 1 and selected for analysis in Section 5. This figure shows the electron distribution parallel and antiparallel to the magnetic field, and the full resolution magnetic field in boundary normal coordinates. The ‘draping only’ FTEs are highlighted in red boxes and numbered D1-4; the ‘core crossing’ FTEs are denoted by purple boxes and numbered C1-9.

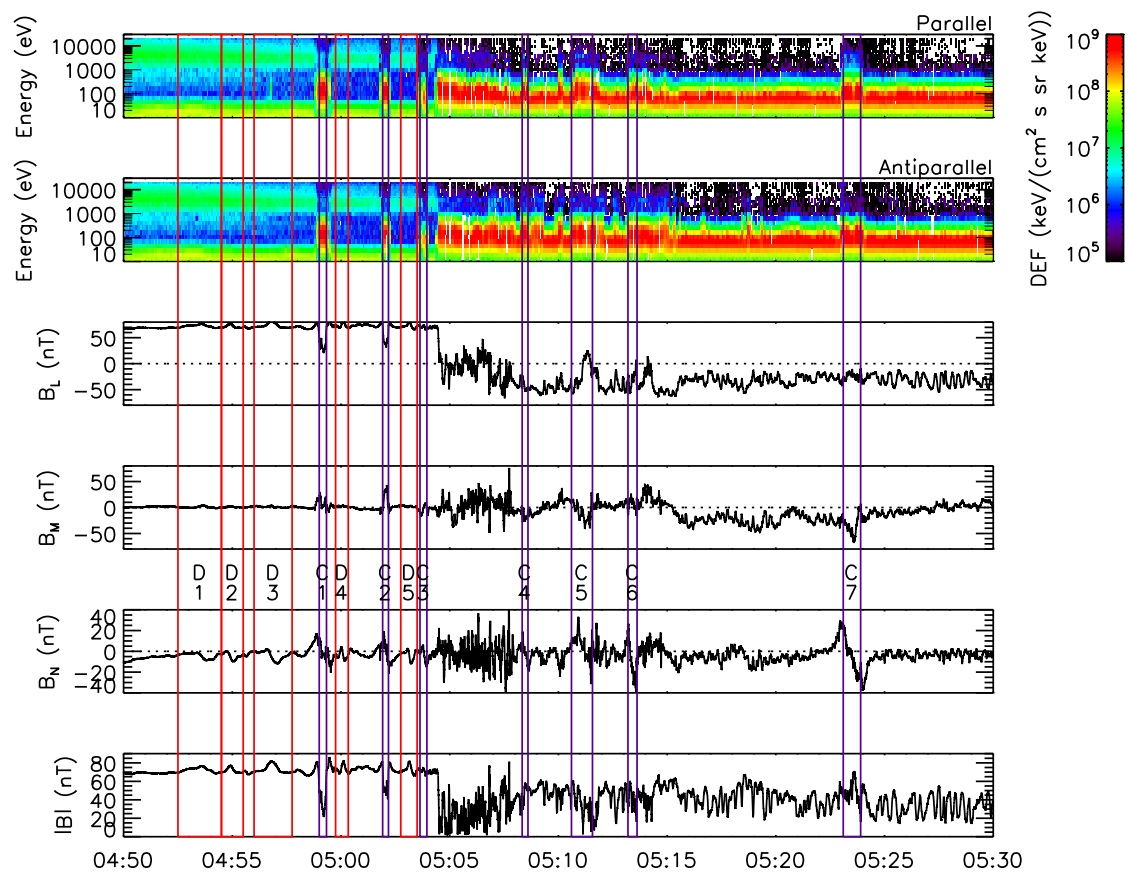


Figure 5: The FTEs observed by Cluster 2 and selected for analysis in Section 5. This figure follows the same format as Figure 4. Note that the FTE numbering at Cluster 2 does not directly map to the numbering at Cluster 1.

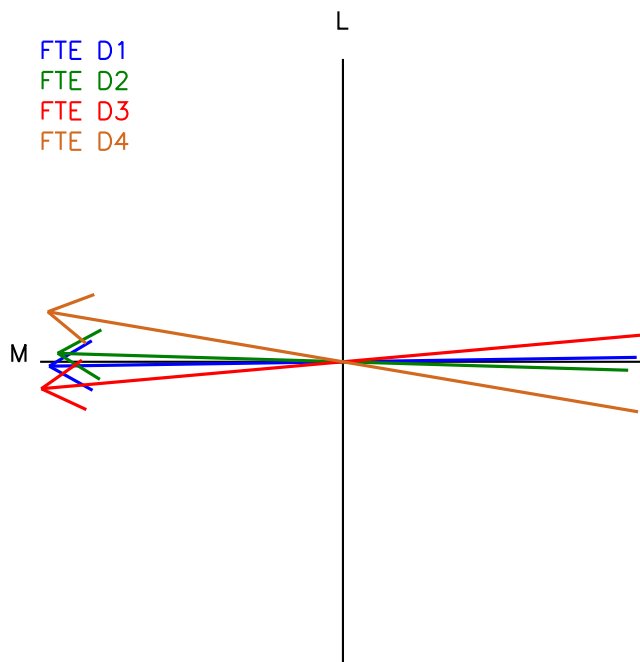


Figure 6: The axes determined by minimum variance analysis, including the correction proposed by *Khrabrov and Sonnerup* (1998), for the ‘draping only’ FTE signatures D1-4 observed by Cluster 1.

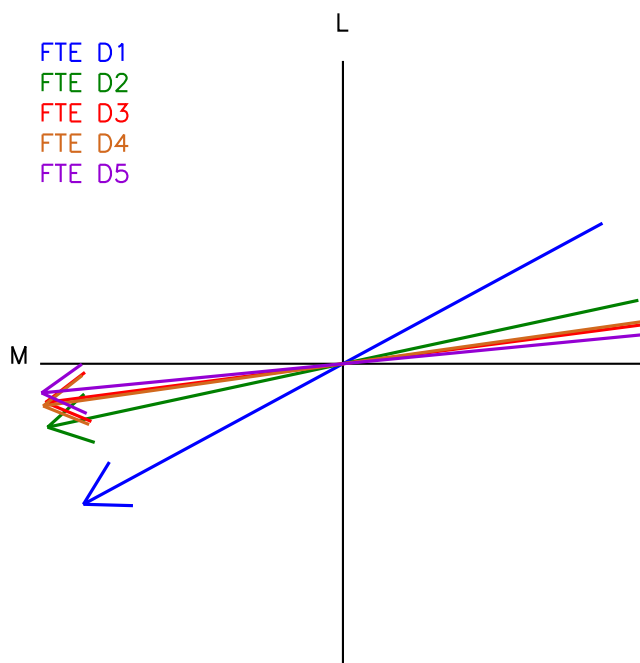


Figure 7: The axes determined by minimum variance analysis, including the correction proposed by *Khrabrov and Sonnerup* (1998), for the ‘draping only’ FTE signatures D1-5 observed by Cluster 2.

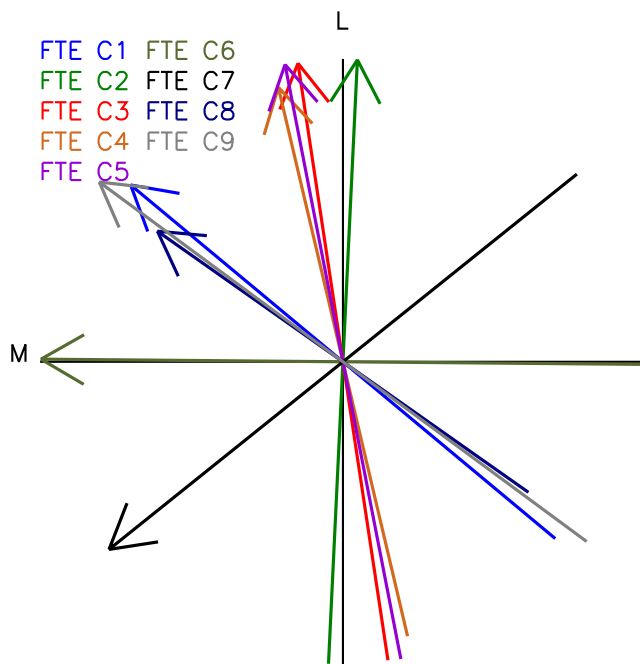


Figure 8: The axes determined by the Faraday's Law method, for the 'core crossing' FTE signatures C1-9 observed by Cluster 1.

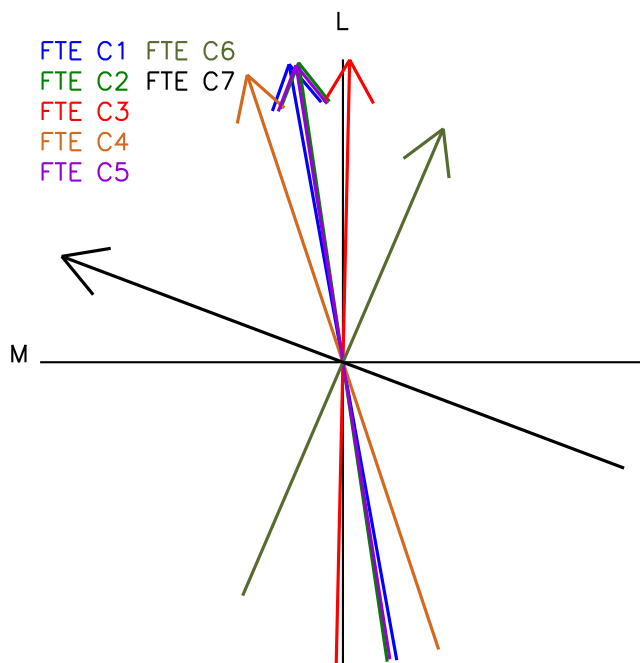


Figure 9: The axes determined by the Faraday's Law method, for the 'core crossing' FTE signatures C1-7 observed by Cluster 2.

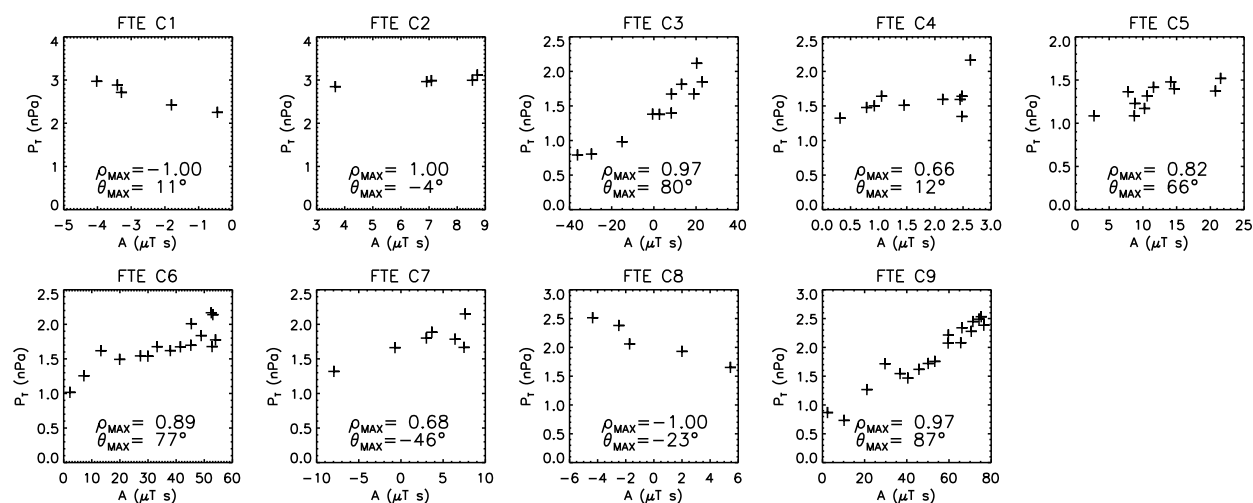


Figure 10: Plots of the total pressure tangential to the axial direction ($P_T = (p_{plasma} + B_z^2/2\mu_0)$) against the magnitude of the magnetic field vector potential (A) for the axial direction (θ) which maximizes the magnitude of the correlation coefficient (ρ_{MAX}). The angle θ lies within the magnetopause plane; $\theta = 0^\circ$ corresponds to an axis along $\hat{\mathbf{i}}$; 90° and 270° correspond to $\pm\hat{\mathbf{m}}$.

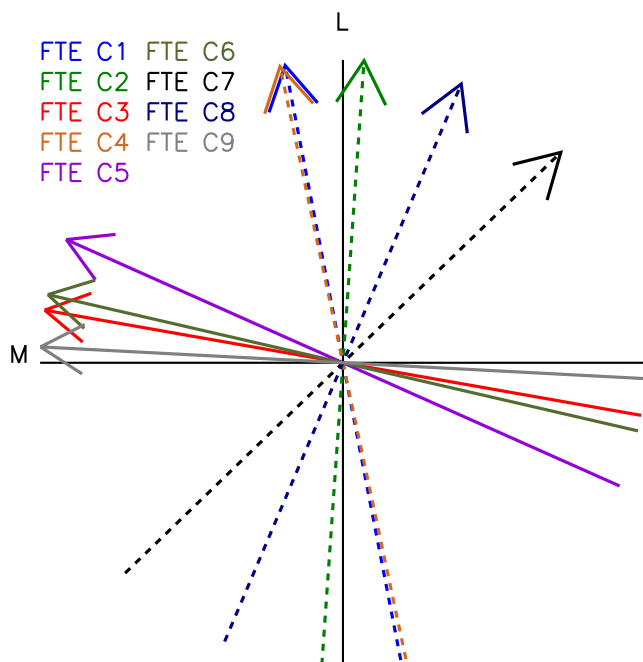


Figure 11: The axes determined by maximising the correlation between P_T and A in the Grad Shafranov method for the ‘core crossing’ FTE signatures C1-9 observed by Cluster 1. Dashed arrows identify intervals with fewer than 10 data points or with a maximum correlation coefficient that was less than 0.7.

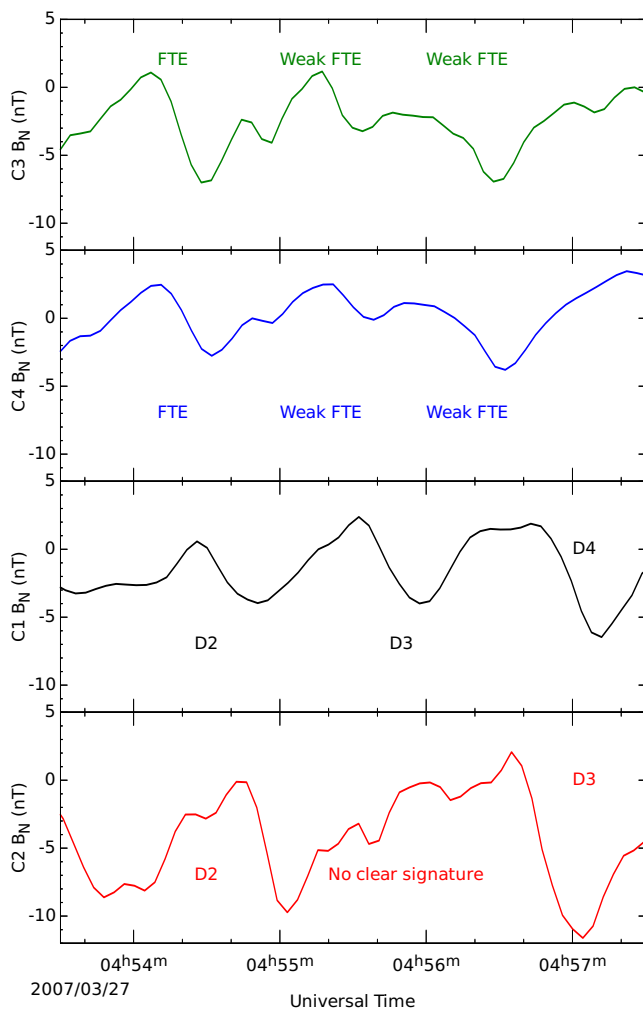


Figure 12: B_N observed by all four spacecraft between 04:54 and 04:58 UT.

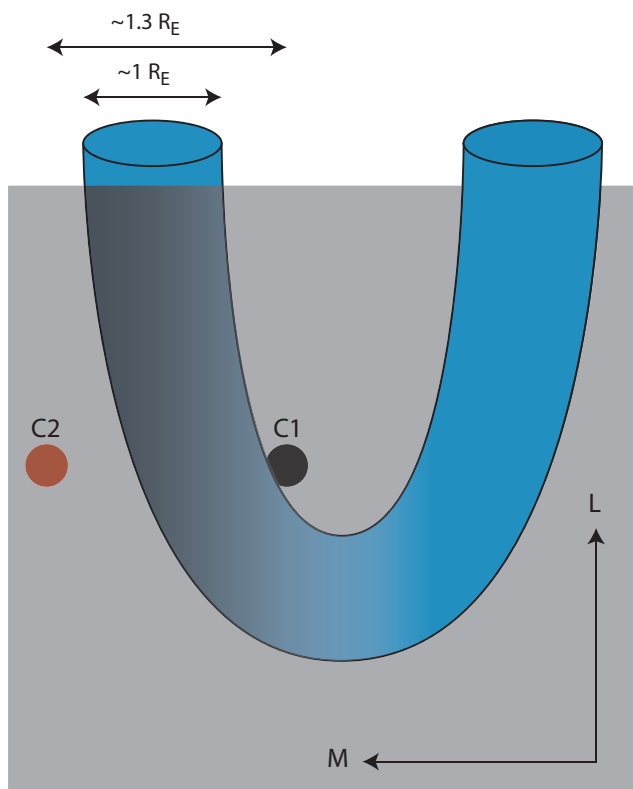


Figure 13: A schematic indicating how ‘patchy’ FTE D3 at Cluster 1 would be interpreted in terms of the *Russell and Elphic (1978)* model if the flux tube had ‘relaxed’ to adopt a more azimuthal orientation as it crossed the magnetopause. The gray plane is the magnetopause, viewed from the magnetosheath. Clusters 1 and 2 are in the magnetosphere, separated by 8,500 km ($1.3 R_E$). If Cluster 1 observes a magnetospheric FTE signature but Cluster 2 (which is closer to the magnetopause) does not, then the *Russell and Elphic (1978)* flux tube must have a poleward orientation within the Cluster tetrahedron, and so Cluster 1 should observe a poleward-directed axis.